APL/JHU CR-24

THE UNIVERSITY OF MICHIGAN

COLLEGE OF ENGINEERING
Department of Aerospace Engineering

CIRCULAR-ARC JET FLAPS AT SUPERSONIC SPEEDS— TWO-DIMENSIONAL THEORY

James L. Amick

ORA Project 06089

under contract with:

THE JOHNS HOPKINS UNIVERSITY
APPLIED PHYSICS LABORATORY
SILVER SPRING, MARYLAND

administered through:

OFFICE OF RESEARCH ADMINISTRATION ANN ARBOR

July 1966

Initial distribution of this report is in accordance with a list on file at the Applied Physics Laboratory, The Johns Hopkins University.

ABSTRACT

An inviscid theory of jet-flap interaction is developed for a two-dimensional jet which issues from a curved nozzle and follows a circular-arc path such that the centrifugal force is in equilibrium with the pressure difference between a high pressure separated flow region along the upstream edge of the jet and a low pressure (base pressure) region along the downstream edge. The theory is based on empirical relations for the pressure in the separated flow region ahead of the jet flap. Results of a large number of numerical calculations are presented to show the effects of the various parameters. The most favorable interaction effects are shown to be associated with laminar separation ahead of weak jets at hypersonic speeds, but even for turbulent separation ahead of a strong jet (lift coefficient = .15) the normal force due to the jet is predicted to approach 7 times the thrust of an ideal jet in a vacuum, when the jet is inclined forward so that it has a substantial upstream component. The theoretical results for circular-arc jet flaps are compared with those for flaps issuing from straight nozzles at the same pressure as that of the upstream separated flow region, and the two types of fully-expanded jets are found to give almost identical results. The lifting efficiency of a jet flap is predicted to compare favorably with that of a flat plate airfoil at angle of attack, for high lift coefficients at hypersonic speeds.

TABLE OF CONTENTS

LIST OF FIGURES

LIST OF SYMBOLS

A axial thrust due to jet flap, per unit span

a_{oj} stagnation speed of sound of jet gas

C_ℓ section lift coefficient $\left(= \dfrac{N_\Delta}{.5\,\gamma_1\,p_1^{\,2}\,L} \right)$

C_t section thrust coefficient $\left(= \dfrac{A}{.5\,\gamma_1\,p_1\,M_1^{\,2}\,L} \right)$

F force acting on portion ACB (Figure 6) of nozzle surface, per unit span

G correction term in the equation $U = U_o - p_b/p_2 + G$

I_{eff} effective specific impulse $\left(= \dfrac{N_\Delta}{m - A/I_{ideal}} \right)$

I_{ideal} ideal specific impulse for discharge into static pressure

$$= a_{oj} \sqrt{\frac{2}{\gamma - 1}} \sqrt{1 - \left(\frac{p_1}{p_{oj}}\right)^{(\gamma - 1)/\gamma}}$$

$I_{ideal\ vac}$ ideal specific impulse in vacuum $\left(= a_{oj} \sqrt{2/(\gamma - 1)} \right)$

I_s specific impulse of normal force $\left(= \dfrac{N_\Delta}{m} \right)$

$I_{s_{vac}}$ specific impulse of normal force in a vacuum $\left(= \dfrac{N_{vac}}{m} \right)$

L distance from jet to effective origin of boundary layer

M_j Mach number along leading edge

M_1 Mach number of flow ahead of jet with jet off

m mass flow rate

N_I	interaction force (resultant of jet-induced pressure changes acting on flat plate ahead of jet), per unit span
N_Δ	total normal force due to jet (including interaction effects), per unit span
N_{vac}	normal force of jet in vacuum, per unit span
p_b	base pressure downstream of jet
p_1	pressure on flat surface ahead of jet with jet off
p_2	pressure in separated flow region ahead of jet
p_{oj}	stagnation pressure of jet gas
R	radius of leading edge of circular-arc jet
Re_L	Reynolds number based on L and flow conditions associated with M_1
r	radial coordinate
S	distance of separation point ahead of jet
U	infinite series in Equation (10)
U_o	value of U when $p_b = 0$
w	width of jet
x	distance to point of boundary layer separation, from effective origin of boundary layer
α	flow separation angle
β	flow intersection angle between jet and main flow
γ	ratio of specific heats of jet gas
γ_1	ratio of specific heats of main stream
δ	jet-flap deflection angle (see Figure 1)
θ	angular coordinate

INTRODUCTION

Jet flaps have been shown to be capable of providing large lift forces at subsonic speeds. At supersonic and hypersonic speeds their capabilities, although less remarkable, appear to be worthy of further investigation.

A jet flap consists of a thin layer of fluid issuing from a trailing-edge slot at an angle to the chord plane (see Figure 1). At subsonic speeds the lift force developed by a jet flap can be an order of magnitude greater than the lift component of the jet momentum. For example, tests of an aspect ratio 3.0 rectangular wing at Mach number 0.85 gave the lift due to a jet flap deflected 90° as approximately 15 times the jet momentum force (Reference 1).

At supersonic speeds most measurements of the lift force due to a jet flap show that the interaction with the main stream magnifies the jet momentum force by a factor of 2 to 4 (References 1-7). However these results are for highly underexpanded jet flaps, where strong shocks in the jet produce large losses in jet momentum. In the present paper, supersonic fully-expanded jet flaps are analysed, and the theoretical results indicate lift forces due to the jet which are considerably larger than the experimental results that have been obtained on highly-underexpanded jet flaps.

The analysis is greatly simplified by considering only a special type of jet flap—that which issues from a curving nozzle such that the constant radius of curvature of the jet provides an equilibrium with the pressure difference between the upstream separation region and the downstream base pressure. Although this is a special case, it should be possible to build

a curving nozzle and obtain results close to those predicted. On the other hand, it is believed that straight nozzles, if operated in the fully expanded mode, can give jet-flap forces comparable to those of the circular-arc jet flap. This is verified for a particular case by a characteristic calculation presented as an appendix to this paper.

The analysis to be presented is similar in many respects to that of Reference 2. However, Reference 2 assumed that the jet flap issuing from any nozzle at any stagnation pressure would somehow be transformed isentropically, after leaving the nozzle, into a circular-arc jet in equilibrium with the pressure difference $p_2 - p_b$. The present analysis avoids this unrealistic assumption, but thereby loses the ability to predict the jet-flap performance as jet stagnation pressure is varied, for a given nozzle. As mentioned above, the present analysis applies only to special nozzles producing circular-arc jets, and operating at jet stagnation pressures that make the exit pressure on the upstream side of the jet equal to p_2; and on the downstream side, equal to p_b.

ANALYSIS

The main features of jet-flap interaction at supersonic speeds are illustrated in Figure 1. In this figure the jet flap is shown as a thin layer of high-velocity gas issuing from a spanwise slot in the lower surface of an airfoil near the trailing edge. For sufficiently large values of the jet deflection angle δ (the angle between the airfoil chord and the jet direction as it leaves the slot), the boundary layer separates upstream of the slot, producing an extensive high pressure region. This high pressure region ahead of the jet causes an interaction force which augments the jet momentum force.

The flow model considered in this analysis is shown in greater detail in Figure 2. Both the jet flow and the main flow are considered to be inviscid, except that the main flow is assumed to separate from the flat surface ahead of the jet at an angle α determined by empirical separation equations, and then to join the jet flow at an intersection angle β, which will be left as a variable of the problem, to be evaluated by future experiments. The jet nozzle is assumed to be so shaped, and the jet stagnation pressure so chosen, that the resulting curved jet follows a circular-arc path in equilibrium with the pressure difference $p_2 - p_b$ between the pressure in the separation region on the upstream side of the jet and the base pressure on the downstream side. Because the jet is in equilibrium, its width remains constant until the deflected main flow intersects with it.

The interaction force N_I is defined as the resultant of jet-induced pressure changes acting on the flat plate ahead of the jet. According to this

simple model

$$N_I = (p_2 - p_1)\, S \tag{1}$$

The separation distance S is related to the jet radius of curvature R as shown in Figure 3. According to this figure

$$\sin \alpha = \frac{a}{S} = \frac{(b + a) - b}{S} = \frac{R \cos\beta - R \cos(\delta - \alpha)}{S}$$

$$S = \frac{R}{\sin \alpha} \left[\cos \beta - \cos (\delta - \alpha) \right] \tag{2}$$

The flow deflection angle α can be determined from the oblique shock relation

$$\alpha = \tan^{-1} \left[\frac{P}{.5\, M_1^2 (\gamma_1 + 1) - P} \sqrt{\frac{M_1^2 - 1 - P}{1 + P}} \right] \tag{3}$$

where

$$P = \frac{(\gamma_1 + 1)}{2\, \gamma_1} (p_2/p_1 - 1).$$

For a flat plate, the pressure ratio p_2/p_1 is given as a function of the Reynolds number at separation by empirical plateau pressure equations (see Reference 2). Thus, for pure laminar separation,

$$\frac{p_2}{p_1} = -1 + 1.27 \sqrt{\frac{M_1^3}{\sqrt{Re_x}}}$$

$$= 1 + 1.27 \sqrt{\frac{M_1^3}{\sqrt{Re_L \frac{(L - S)}{L}}}} \tag{4}$$

where L is the distance from the flat plate leading edge (or equivalent origin of the boundary layer) to the leading edge of the jet slot; and Re_L is Reynolds number based on L and the conditions associated with p_1 and M_1. Similarly,

for turbulent separation, the plateau pressure (or first peak pressure) can be approximated by (see Reference 2)

$$\frac{p_2}{p_1} = 1 + 2.6 \frac{\sqrt{M_1^2 - 1}}{(Re_x)^{1/10}}$$

$$= 1 + 2.6 \frac{\sqrt{M_1^2 - 1}}{(Re_L)^{1/10}} \left(\frac{L}{L - S} \right)^{1/10} \qquad (5)$$

Equations (4) and (5) can be solved for S/L to give, for laminar separation

$$\frac{S}{L} = 1 - \frac{2.60}{(p_2/p_1 - 1)^4} \frac{M_1^6}{Re_L} \qquad (6)$$

and, for turbulent separation

$$\frac{S}{L} = 1 - \frac{14{,}100 \, (M_1^2 - 1)^5}{(p_2/p_1 - 1)^{10} \, Re_L} \qquad (7)$$

The relation between the jet width and its radius of curvature is a function of the pressures p_2 and p_b, as can be seen by considering the balance of forces on a fluid element of the jet. Thus, the radial pressure gradient across a fluid element of area $(rd\theta)\,(dr)$ must balance the centrifugal force:

$$(rd\theta)\, dp = \frac{\rho \, (rd\theta) \, (dr) \, V^2}{r} \qquad (8)$$

For isentropic flow of a perfect gas this equation integrates to

$$\frac{w}{R} = 1 - \sqrt{\frac{1 - \left(\frac{p_2}{p_{oj}} \right)^{(\gamma - 1)/\gamma}}{1 - \left(\frac{p_b}{p_{oj}} \right)^{(\gamma - 1)/\gamma}}} \qquad (9)$$

where γ is the ratio of specific heats of the jet gas.

The mass flow of the circular-arc jet (per unit span) was found in Reference 2 to be

$$\dot{m} = \frac{p_2 R \sqrt{1 - \left(\frac{p_2}{p_{oj}}\right)^{(\gamma - 1)/\gamma}}}{a_{oj}\sqrt{2/(\gamma - 1)}} \Bigg/ \frac{p_2}{p_{oj}} \int_{p_b/p_{oj}}^{p_2/p_{oj}} \frac{dz}{1 - z^{(\gamma - 1)/\gamma}}$$

$$= \frac{p_2 R U}{a_{oj}\sqrt{2/(\gamma - 1)}} \tag{10}$$

where a_{oj} is the stagnation speed of sound of the jet gas, and

$$U \equiv \sum_{n=1}^{\infty} a_n \left(p_2/p_{oj}\right)^{(n - 1)(\gamma - 1)/\gamma}$$

$$a_1 \equiv 1 - p_b/p_2$$

$$a_2 \equiv \frac{\gamma}{2\gamma - 1}\left[1 - \left(\frac{p_b}{p_2}\right)^{(2\gamma - 1)/\gamma}\right] - \frac{1}{2}\left(1 - \frac{p_b}{p_2}\right)$$

$$a_3 \equiv \frac{\gamma}{3\gamma - 2}\left[1 - \left(\frac{p_b}{p_2}\right)^{(3\gamma - 2)/\gamma}\right] - \frac{1}{2}\frac{\gamma}{(2\gamma - 1)}\left[1 - \left(\frac{p_b}{p_2}\right)^{(2\gamma - 1)/\gamma}\right]$$

$$- \frac{1}{2 \cdot 4}\left(1 - \frac{p_b}{p_2}\right)$$

$$a_4 \equiv \frac{\gamma}{4\gamma - 3}\left[1 - \left(\frac{p_b}{p_2}\right)^{(4\gamma - 3)/\gamma}\right] - \frac{1}{2}\frac{\gamma}{(3\gamma - 2)}\left[1 - \left(\frac{p_b}{p_2}\right)^{(3\gamma - 2)/\gamma}\right]$$

$$- \frac{1}{2 \cdot 4}\frac{\gamma}{(2\gamma - 1)}\left[1 - \left(\frac{p_b}{p_2}\right)^{(2\gamma - 1)/\gamma}\right] - \frac{1 \cdot 3}{2 \cdot 4 \cdot 6}\left(1 - \frac{p_b}{p_2}\right)$$

$$\vdots \quad a_n \equiv \sum_{i=1}^{n} \frac{(2i)!\ 2i\ \gamma \left[1 - \left(\frac{p_b}{p_2}\right)^{[(n-1)(\gamma-1)+\gamma]/\gamma} \right]}{2^{2i}\,(i!)^2(2i-1)(3-2i)\left[(n-i)(\gamma-1)+\gamma\right]}$$

For small values of p_2/p_{oj} the infinite series U converges quite rapidly, so that only a few terms are needed. Values of the sum of the first five terms of the series are shown in Figure 4 for $p_b = 0$, along with exact values of the series calculated from closed-form expressions which exist for particular values of γ expressible in the form $\gamma = (N + 2)/N$, where N is an integer. (The closed-form expressions for U contain the difference of two nearly-equal large numbers, for small values of p_2/p_{oj}, so that the series expression is usually more convenient.) The use of only five terms of the series should give an adequate representation of U_o for most cases of practical interest.

A convenient relation between the value U_o of U for zero base pressure and the value of U for some finite base pressure at the same γ and p_2/p_{oj} (or M_j) is

$$U = U_o - p_b/p_2 + G \tag{11}$$

The correction term G is usually small, as shown in Figure 5.

The jet force is obtained by reference to Figure 6. The force due to pressures acting on a portion of the nozzle surface ACB is

$$F = \int_{R-w}^{R} (p + \rho V^2)\, dr$$

But from Equation (8)

$$\rho V^2 dr = r dp$$

Then

$$F = \int_{R-w}^{R} pdr + rdp = \int_{P_b(R-w)}^{p_2 R} d(pr)$$

$$= p_2 R - p_b (R - w) \tag{12}$$

The force F acts at an angle δ to the airfoil surface.

The remainder of the nozzle surface (the arc BD) is acted on by base pressure. The normal component of the force on BD is

$$N_{BD} = p_b \, (w' - w \sin \delta) \tag{13}$$

where

$$w' = \overline{AN} - \overline{DN} = \overline{AN} - \sqrt{\overline{OD}^2 - \overline{ON}^2}$$

$$= R \sin \delta - \sqrt{(R - w)^2 - (R \cos \delta)^2}$$

$$= R\left[\sin \delta - \sqrt{\left(1 - \frac{w}{R}\right)^2 - \cos^2 \delta}\right] \tag{14}$$

Then the normal force due to pressures acting over the entire nozzle surface (which also is the normal force in a vacuum) is

$$N_{vac} = R \left[p_2 \sin \delta - p_b \sqrt{\left(1 - \frac{w}{R}\right)^2 - \cos^2 \delta}\right] \tag{15}$$

The corresponding specific impulse is

$$I_{s_{vac}} = \frac{N_{vac}}{\dot{m}}$$

$$= \frac{a_{oj}}{U} \sqrt{2/(\gamma - 1)} \left[\sin\delta - \frac{p_b}{p_2} \sqrt{\left(1 - \frac{w}{R}\right)^2 - \cos^2 \delta}\right] \tag{16}$$

Now the total normal force due to the jet (the difference between jet-on

and jet-off pressures acting over all nozzle and airfoil surfaces) can be written

$$N_\Delta = N_I + N_{vac} - p_1 w'$$

$$= R\left[\frac{(p_2 - p_1)(\cos\beta - \cos\delta\cos\alpha)}{\sin\alpha} + (p_1 - p_b)\sqrt{(1 - \frac{w}{R})^2 - \cos^2\delta}\right] \quad (17)$$

The axial thrust due to the jet is obtained by adding the axial components of F and the force acting on BD:

$$A = R\left[p_2\cos\delta - p_b(1 - \frac{w}{R})\cos\delta - p_b\frac{w}{R}\cos\delta\right]$$

$$= R(p_2 - p_b)\cos\delta \quad (18)$$

The specific impulse of the jet flap can now be written, by combining (10) and (17), as

$$I_s = \frac{N_\Delta}{\dot{m}}$$

$$= \frac{a_{oj}}{U}\sqrt{2/(\gamma - 1)}\left[(1 - \frac{p_1}{p_2})(\frac{\cos\beta - \cos\delta\cos\alpha}{\sin\alpha}) + (\frac{p_1}{p_2} - \frac{p_b}{p_2})\sqrt{(1 - \frac{w}{R})^2 - \cos^2\delta}\right] \quad (19)$$

For comparison, the specific impulse of the same gas exhausting through an ideal nozzle into a vacuum is

$$I_{ideal\ vac} = a_{oj}\sqrt{2/(\gamma - 1)} \quad (20)$$

so that the ratio of the actual specific impulse of the normal force to the

specific impulse of an ideal nozzle is

$$\frac{I_s}{I_{ideal\ vac}} = \frac{1}{U}\left[\left(1 - \frac{p_1}{p_2}\right)\left(\frac{\cos\beta - \cos\delta\cos\alpha}{\sin\alpha}\right) + \left(\frac{p_1}{p_2} - \frac{p_b}{p_2}\right)\sqrt{\left(1 - \frac{w}{R}\right)^2 - \cos^2\delta}\right] \tag{21}$$

For some applications the axial force, as well as the normal force, may be of importance. Then the specific impulse should include not only the actual mass flow of the jet flap, but also the mass flow of a propulsive jet needed to overcome any negative thrust due to a forward-inclined jet flap. If the jet flap is inclined toward the rear, then the mass flow for specific impulse purposes should consist of the actual jet-flap mass flow minus the reduction in mass flow of the propulsive jet due to the thrust component of the jet flap.

Accordingly, an effective specific impulse will be defined as the total normal force due to the jet, divided by the mass flow of the jet plus (minus) the mass flow required to overcome the rearward (forward) axial force due to the jet, using an ideal nozzle to generate thrust with the same gas. In this case the ideal nozzle will exhaust into the free stream static pressure, with a specific impulse of

$$I_{ideal} = a_{oj}\sqrt{2/(\gamma - 1)}\sqrt{1 - (p_1/p_{oj})^{(\gamma - 1)/\gamma}} \tag{22}$$

The effective specific impulse according to the above definition is

$$I_{eff} = \frac{N_\Delta}{\dot{m} - A/I_{ideal}}$$

This quantity was also used by Maurer (Reference 5) as a measure of the

efficiency of a side jet, in the nondimensional form

$$c_n \equiv I_{eff}/I_{ideal}$$

For a circular-arc jet flap the effective specific impulse resulting from the above definition is

$$I_{eff} = \frac{a_{oj}\sqrt{2/(\gamma-1)}\left[(1-\frac{p_1}{p_2})(\frac{\cos\beta-\cos\delta\cos\alpha}{\sin\alpha})+(\frac{p_1}{p_2}-\frac{p_b}{p_2})\sqrt{(1-\frac{w}{R})^2-\cos^2\delta}\right]}{U-(1-p_b/p_2)\cos\delta/\sqrt{1-(p_1/p_{oj})^{(\gamma-1)/\gamma}}} \tag{23}$$

The nondimensional effective specific impulse is

$$\frac{I_{eff}}{I_{ideal\ vac}} = \frac{(1-\frac{p_1}{p_2})\frac{\cos\beta-\cos\delta\cos\alpha}{\sin\alpha}+\frac{p_1}{p_2}(1-\frac{p_b}{p_1})\sqrt{(1-\frac{w}{R})^2-\cos^2\delta}}{U-(1-p_b/p_2)\cos\delta/\sqrt{1-(p_1/p_{oj})^{(\gamma-1)/\gamma}}} \tag{24}$$

A section lift coefficient may be defined as

$$c_\ell = \frac{N_\Delta}{.5\,\gamma_1\,p_1\,M_1^2\,L} \tag{25}$$

where a zero angle of attack is presupposed, so that the normal to the airfoil surface is also normal to the undisturbed air stream. When (2) and (17) are substituted into (25), there results

$$C_\ell = \frac{S}{L}\frac{2}{\gamma_1 M_1^2}\frac{\left[(\frac{p_2}{p_1}-1)(\cos\beta-\cos\delta\cos\alpha)+\sin\alpha\,(1-\frac{p_b}{p_1})\sqrt{(1-\frac{w}{R})^2-\cos^2\delta}\right]}{(\cos\beta-\cos\delta\cos\alpha-\sin\delta\sin\alpha)} \tag{26}$$

The preceeding equations can be solved for given values of jet Mach number (which determines p_2/p_{oj}) and p_2/p_1. Equation (3) is used to find α. Depending on the boundary layer condition, Equation (6) or (7) gives S/L. For an assumed value of p_b/p_1, w/R is evaluated from Equation (9) and the

infinite series is determined from Figure 4 and 5 and Equation (11). The specific impulse ratios and lift coefficient can then be found, for a chosen value of β, from Equations (21), (24), and (26).

In the following section these equations are used to obtain numerical results which illustrate the effects of the various parameters.

CALCULATED RESULTS AND DISCUSSION

The equations developed in the preceeding section present no essential difficulty to hand calculation. However, they were programmed for the IBM 7090 computer in order that a large number of cases could be calculated at little cost. Approximately 6000 cases were thus calculated in about 5 minutes of machine time, producing the results which are presented in the remainder of this report.

The variation of specific impulse with the lift coefficient based on the total normal force due to the jet is presented in Figure 7 for five different combinations of free-stream Mach number and jet-flap deflection angle. In this figure and in most of the following ones the Mach number at the leading edge of the jet (M_j) is 8.0, the jet specific heat ratio (γ) is 1.4, the base pressure (p_b) is .3 of the stream static pressure (p_1), and the Reynolds number (Re_L) based on distance from the jet to the effective origin of the boundary layer is 10 million.

Results are shown for several different values of β, the flow intersection angle. It is expected that for most cases the proper value of β would lie within the range of values shown. This range of β represents a 20-30% uncertainty in specific impulse, for $\delta = 90°$.

It should be emphasized that the variation in lift coefficient, for a given β, shown in this report is obtained not by varying the jet stagnation pressure but by varying the width of the nozzle producing the jet. Each β =

constant curve therefore represents the performance of a series of different-sized jet-flap nozzles. The present report contains no information on the variation in performance as jet stagnation pressure ratio is varied for a given configuration.

Curves for both laminar and turbulent separation are shown in Figure 7. For very weak jets laminar separation gives approximately twice as much specific impulse as does turbulent separation. However, this advantage of laminar separation over turbulent separation decreases rapidly as the jet strength is increased, and when the separation point nears the leading edge the difference between the two types of separation vanishes.

The jet width w/L is shown as a parameter in the plots of Figure 7. In Figure 8 the plateau pressure rise at separation (p_2/p_1) is presented as a function of w/L. Knowing p_2/p_1, it is relatively easy to calculate any of the other parameters that might be of interest, from the equations of the preceeding section. For instance, the value of w/R can be obtained from Equation (9), since having p_2/p_1 enables p_b/p_{oj} to be calculated from the given values of p_2/p_{oj} and p_b/p_1.

The effect of free-stream Mach number (M_1) on the specific impulse of jet flaps is shown in Figure 9 for a jet deflection of 90°. For very weak jets (as represented in the limit by $C_\ell = 0$) the specific impulse increases greatly with Mach number. However for strong jets ($C_\ell = .15$) the effect of Mach number becomes much less.

The flat-plate curve shown in Figure 9 (b) is based on a flat-plate airfoil at angle of attack, where the specific impulse is calculated as the

lift of the wing divided by the mass flow of an ideal nozzle that provides a thrust equal to the drag-due-to-lift of the airfoil. That is

$$I_{s_{\text{Flat plate}}} = \frac{\text{Lift}}{\text{Drag-due-to-lift} / I_{\text{ideal vac}}}$$

Then the specific impulse ratio of the flat-plate airfoil is merely its lift-to-drag ratio. The lift-drag ratios shown for the flat plate were calculated by the shock-expansion method, with skin friction neglected.

The comparison between airfoils with jet flaps deflected 90° and the flat-plate airfoil at angle of attack, shown in Figure 9 (b), indicates comparable lifting efficiency for the two systems at high lift coefficients and hypersonic speeds. A similar comparison will be presented later for optimum jet-flap deflection angles.

Similar effects of free-stream Mach number are shown in Figure 10, for the case of jet flaps deflected 150°. For this deflection angle the specific impulse values are about twice as large as those for a deflection angle of 90°. However, in the case of the 150° deflection there is an additional drag due to the forward-directed component of the jet, which must be considered.

The variation of specific impulse with jet-flap deflection angle δ is presented in Figure 11, for a free-stream Mach number of 8.0. Again it should be remembered that for jet-flap deflection angles greater than 90° the forward-directed component of the jet momentum represents a drag force; for angles less than 90°, the rearward-directed momentum gives thrust. The curves are generally sinusoidal, with the specific impulse varying roughly as the sine squared of half the jet-flap deflection angle.

Jet-Mach-number effects are shown in Figure 12. For hypersonic jet Mach numbers, specific impulse increases only slightly with jet Mach number. In all cases the variation of specific impulse is quite similar to that of the vacuum specific impulse, as shown by comparison of the short-dashed curves with the corresponding solid or broken curves. This similarity means that increases in jet momentum due to increasing jet Mach number are accompanied by almost-proportional increases in the interaction force. However, Maurer (Reference 5) predicted that the interaction force would be unaffected by the jet Mach number, whereas Vinson (Reference 7) predicted an increase in interaction force with jet Mach number considerably in excess of that which would be proportional to the jet momentum.

The effect of jet gas specific heat ratio γ, shown in Figure 13, is small, as was also found by Maurer. It should be noted, however, that the jet gas specific heat ratio also affects the ideal specific impulse $I_{\text{ideal vac}}$, which is the denominator in the specific impulse ratio plotted in Figure 13. For a γ of 1.1 the value of $I_{\text{ideal vac}}$ is twice that for a γ of 1.4, so that the trend of the variation of specific impulse (I_s) with γ is opposite to that shown in Figure 13 for the specific impulse ratio ($I_s/I_{\text{ideal vac}}$). The specific impulse itself would actually decrease by almost a factor of 2 in going from $\gamma = 1.1$ to $\gamma = 1.4$.

Curves proportional to the vacuum specific impulse are also shown on Figure 13. (Where no short-dashed curve is shown it is identical to the corresponding solid or broken curve.) Again, as in the case of the jet Mach number, changes in jet momentum due to varying γ cause nearly-proportional

changes in the interaction force.

The stagnation speed of sound (a_{0j}) of the jet gas has a similar effect on specific impulse. Although the specific impulse ratio $I_s/I_{ideal\ vac}$ is independent of a_{0j}, both I_s and $I_{idealvac}$ are directly proportional to a_{0j}.

Reynolds number effects are presented in Figure 14. The largest effects of Reynolds number on specific impulse are indicated for weak jets and laminar separation. For strong jets, where the separation point is near the leading edge, the Reynolds number effect, as well as the effect of type of separation (laminar or turbulent) becomes vanishingly small.

The theory for circular-arc jet flaps developed in the preceeding section requires that the base pressure p_b on the downstream side of the jet be known or assumed. The effect of this base pressure assumption on specific impulse is shown in Figure 15. When the pressure p_2 on the upstream side of the jet is relatively small, as for a weak jet with laminar separation, then the base pressure assumption has its largest effect on specific impulse. On the other hand, for relatively large values of p_2, associated with turbulent separation or strong jets, the base pressure effect is quite small.

The remaining comparisons to be presented show the effects of flap deflection, free-stream Mach number, and lift coefficient on the effective specific impulse as defined in the preceeding section. This effective specific impulse includes the additional mass flow of a propulsive jet required to neutralize the drag component of the jet momentum when the jet has a deflection angle greater than 90°. Similarly, when the jet deflection angle is less than 90° the mass flow used in calculating the effective specific impulse is reduced

by the mass-flow equivalent of the thrust component of the jet flap.

The effect of jet-flap deflection angle on the effective specific impulse is presented in Figure 16 for a free-stream mach number of 8.0. For small values of δ no separation occurs ahead of the jet, and the effective specific impulse decreases rapidly with increasing δ approximately as the relation $I_{eff}/I_{ideal\ vac} = \sin\delta / (1 - \cos\delta)$. (For an ideal nozzle exhausting from the base of an airfoil in a vacuum with a force F inclined at an angle δ to the chord the effective specific impulse ratio would be

$$\frac{I_{eff}}{I_{ideal\ vac}} = \frac{F \sin\delta}{(\dot{m} - F\cos\delta / I_{ideal})\, I_{ideal\ vac}} = \sin\delta / (1 - \cos\delta).$$

The no-separation line shown in Figure 16 (a) is in quite close agreement with this approximate relationship.)

As δ increases a value is reached, depending on β, at which separation begins to occur ahead of the jet. Further increase in δ then causes a rapid rise in effective specific impulse, as the effectiveness of the jet in producing separation increases.

When the section lift coefficient produced by the jet flap is held constant at $C_\ell = .15$, then very large nozzles are required at the low flap deflection angles, as indicated in Figure 16 (b) by the comparatively large values of the jet width parameter w/L in the vicinity of the no-separation line. The large values of w/L are accompanied by large values of the thrust coefficient C_t, defined by

$$C_t \equiv \frac{A}{.5\,\gamma_1 M_1^2 p_1 L}.$$

If the thrust of the jet flap becomes larger than the thrust required of the main propulsion system, then the effective specific impulse loses its significance as a measure of efficiency.

Because of the large nozzle sizes and thrust coefficients required for jet-flap configurations at small-enough flap deflection angles to avoid separation, only configurations which produce separation ahead of the jet flap will be considered in the remaining comparisons of effective specific impulse.

The optimum flap deflection angle (i.e., that which produces the largest effective specific impulse at a given value of β) varies considerably with β, C_ℓ, etc., as shown in Figure 16. However, the effective specific impulse for any deflection angle between 90° and 160° is generally not much less than the effective specific impulse at the optimum flap deflection angle, except for extreme values of β. Therefore, the large forces that are predicted for large flap deflection angles (for example, δ = 150°, Figures 7 (e) and 10) usually involve only small sacrifices in lifting efficiency.

The variation of effective specific impulse with section lift coefficient is shown in Figure 17 for several different flap deflection angles, at a free-stream Mach number of 8.0 and a flow intersection angle of 25°. The several flap deflection curves form an envelope curve of optimum flap deflection, which is plotted in Figure 18 along with similar envelope curves for three other β values. For each β value at sufficiently high lift coefficients there are jet-flap configurations which give greater lifting efficiency than does a flat-plate airfoil.

The effect of free-stream Mach number on the effective specific impulse of jet flaps having optimum deflection angles is presented in Figure 19 for two different lift coefficients. For weak jets ($C_\ell = 0$) the effective specific impulse increases greatly with free-stream Mach number. However, for strong jets ($C_\ell = .15$) the Mach number effect is very small for laminar separation and for turbulent separation at the higher Mach numbers. For $\beta = 25°$ and $C_\ell = .15$ the jet flap compares favorably with the flat plate at Mach numbers above 10.

The circular-arc jet flap is compared in Figure 20 with a straight jet flap (see the Appendix). The two types of jet flap give almost identical results, perhaps because both jet flows were treated as shock-free. (The circular-arc jet actually is shock-free, and the straight jet calculation was simplified by treating its shock as an isentropic compression.) The similarity of the results for these two types of fully-expanded jet flaps suggests that the preceding results for circular-arc jet flaps may be typical of jet flaps using other types of nozzles, as long as the static pressure at the nozzle exit matches the pressure in the separated flow upstream of the jet.

Some caution should be exercised in using the theoretical results presented herein, since experimental checks on the adequacy of the theoretical flow model are not yet available. It is conceivable that viscous effects could have an important influence on the effective shape of the jet. Also, variations of pressure in the separated flow region could cause the actual interaction flow pattern to differ significantly from the theoretical pattern based on constant pressure.

CONCLUSIONS

The following conclusions are based on the preceeding theoretical results for circular-arc jet flaps, but they may also apply to other two-dimensional jet-flap configurations where the jet-exit static pressure matches the pressure in the separation region just upstream of the jet (i.e., fully-expanded jets):

1. Normal forces as large as 15 to 25 times the thrust of an ideal nozzle in a vacuum are predicted for weak jet flaps directed upstream and producing laminar separation at hypersonic free-stream speeds.

2. Laminar separation ahead of weak jet flaps results in values of normal force specific impulse that are approximately twice as large as those for turbulent separation. When jet flaps of different strength are compared, relatively small decreases in specific impulse with increasing jet strength are noted for turbulent separation, whereas the decreases for laminar separation are large. The difference in specific impulse between laminar and turbulent separation decreases with increasing jet strength, becoming small when the separation point reaches the vicinity of the leading edge.

3. Free-stream Mach number increases cause large increases in the specific impulse values of weak jet flaps. On the other hand, for strong jet flaps there is not much change in specific impulse above a Mach number of 8.0.

4. The inclination of a jet flap affects specific impulse approximately

as the square of the sine of half the jet-flap deflection angle.

5. Jet gas properties have important effects on specific impulse. The specific impulse is proportional to the stagnation speed-of-sound of the jet gas, and is approximately doubled by a decrease in jet gas specific heat ratio from 1.4 to 1.1.

6. Jet Mach number increases cause moderate increases in specific impulse, up to jet Mach numbers of about 6. At hypersonic jet Mach numbers there is little further increase in specific impulse with increasing jet Mach number.

7. Reynolds number and base pressure generally have little effect on specific impulse. Their largest effects are associated with laminar separation ahead of weak jets, and even then a 20% increase in specific impulse requires an order of magnitude increase in Reynolds number or an increase in base pressure of approximately one quarter of the free stream static pressure.

8. In lifting efficiency, jet flaps are comparable with a flat plate airfoil at angle of attack, for high lift coefficients at hypersonic speeds.

9. Lifting efficiency is only slightly reduced when the flap deflection angle is increased beyond the optimum, and such an increase can provide a large increase in normal force specific impulse.

REFERENCES

1. Poisson-Quinton, Ph., and Lepage, L.: French Research on Control of Boundary Layer and Circulation. In "Boundary Layer and Flow Control, Vol. I," edited by C. V. Lachmann, Pergamon Press, 1961.

2. Amick, J. L., and Carvalho, G. F.: Interaction Effects of a Jet Flap on a 60° Delta Wing at Mach Number 4, and Comparison with Two-Dimensional Theory. University of Michigan Dept. of Aerospace Engineering Report APL/JHU CM-1031, February 1963.

3. Strike, W. T., Schueler, C. J., and Deitering, J. S.: Interactions Produced by Sonic Lateral Jets Located on Surfaces in a Supersonic Stream. AEDC-TDR-63-22, April 1963.

4. Heyser, A., and Maurer, F.: Experimental Investigations on Solid Spoilers and Jet Spoilers at Mach Numbers of .6 to 2.8. JPL/CIT, Translation No. 32, February 1964, or Zeitschrift fur Flugwissenschaften, V. 10, No. 4,5, 1962.

5. Maurer, F.: Interference Effects Produced by Gaseous Side-Jets Issuing into a Supersonic Stream. APL/JHU TG 230-T460, November 1965, translated by L. J. Holtschlag from DVL-Bericht No. 382, January 1965.

6. Hawk, N. E., and Amick, J. L.: An Experimental and Theoretical Investigation of Two-Dimensional Jet-Flap Aerodynamic Interaction at Supersonic Speeds. University of Michigan Dept. of Aerospace Engineering Report APL/JHU CR-23, October 1965.

7. Vinson, P. W.: Prediction of Reaction Control Effectiveness at Supersonic and Hypersonic speeds. Martin-Orlando OR 6487, March 1965.

APPENDIX

TWO-DIMENSIONAL THEORY OF STRAIGHT JET FLAPS

A straight jet flap is a uniform, parallel jet issuing from a slot-nozzle near the trailing edge with a static pressure equal to that of the separated flow region just ahead of it. Because of the balanced pressures on the upstream edge of the jet, that edge is straight for a certain distance. At the downstream corner of the nozzle the jet flow turns to expand to the base pressure. Expansion waves from this Prandtl-Meyer turn cross the jet, reaching the upstream edge of the jet at some distance from the nozzle exit, and causing that edge to curve toward the downstream direction.

A simplified model of the interaction of a straight jet flap with a supersonic stream is shown in Figure 21. As seen from this figure, the angle of turning of the upstream edge of the jet is

$$\Phi = \delta - \beta - \alpha \tag{27}$$

The separation distance is related to the jet width by

$$S = \frac{\sin(\delta - \alpha)}{\sin \alpha} \left[h + \frac{w}{\tan \delta} - \frac{g}{\tan(\delta - \alpha)} \right]$$

$$= w \sin \delta \left[\left(\frac{h}{w} + \cot \delta \right) (\cot \alpha - \cot \delta) - \frac{g}{w} (\cot \alpha \cot \delta + 1) \right] \tag{28}$$

The quantities h/w and g/w can be found as functions of Φ by means of a graphical construction of the jet shape. Such a construction, utilizing the method of characteristics, is shown in Figure 22 for a jet Mach number

of $M_j = 4.0$, a base pressure of $p_b = .004\ p_2$, and a value of γ of 1.4. (The expansion fan was approximated by finite expansion waves across which the flow direction turned 2°. The shock wave (formed by the coalescence of the compression waves produced by reflection of the expansion waves at the upstream constant-pressure edge of the jet) was treated as an isentropic compression.)

The normal force in a vacuum is

$$N_{vac} = wp_2 \left[1 + \gamma M_j^2\right] \sin\delta + wp_2 \frac{\cos^2\delta}{\sin\delta} \tag{29}$$

$$= wp_2 \left[\frac{1}{\sin\delta} + \gamma M_j^2 \sin\delta\right]$$

so that the total normal force due to the jet is

$$N_\Delta = N_t + N_{vac} - p_1\, w/\sin\delta$$

$$= wp_2 \sin\delta \left\{\left(1 - \frac{p_1}{p_2}\right) \left[\frac{h}{w} (\cot\alpha - \cot\delta) + \left(1 - \frac{g}{w}\right)(\cot\alpha \cot\delta + 1)\right] + \gamma M_j^2\right\} \tag{30}$$

The mass flow is

$$\dot{m} = \frac{wp_2\, \gamma\, M_j}{a_{oj}} \sqrt{1 + \frac{\gamma - 1}{2} M_j^2}$$

and from this the specific impulse ratio is obtained as

$$\frac{I_s}{I_{ideal\ vac}} = \frac{N_\Delta}{\dot{m}\, a_{oj}\, \sqrt{2/(\gamma - 1)}}$$

$$= \frac{\sin \delta}{\gamma M_j \sqrt{M_j^2 + 2/(\gamma - 1)}} \left\{ \gamma M_j^2 + \left(1 - \frac{p_1}{p_2}\right) \left[\frac{h}{w}(\cot \alpha - \cot \delta) + \left(1 - \frac{g}{w}\right)(\cot \alpha \cot \delta + 1) \right] \right\} \quad (31)$$

The lift coefficient is obtained by solving (28) for w and combining with (30)

$$C_\ell = \frac{\frac{S}{L} \left\{ \left(1 - \frac{p_1}{p_2}\right) \left[\frac{h}{w} (\cot \alpha - \cot \delta) + \left(1 - \frac{g}{w}\right)(\cot \alpha \cot \delta + 1) \right] + \gamma M_j^2 \right\}}{\frac{\gamma_1}{2} M_1^2 \frac{p_1}{p_2} \left[\left(\frac{h}{w} + \cot \delta\right)(\cot \alpha - \cot \delta) - \frac{g}{w} (\cot \alpha \cot \delta + 1) \right]} \quad (32)$$

The procedure for solving these equations is similar to that for the circular-arc jet flap: A value of p_2/p_1 is chosen, and Equations (3) and (6) or (7) are used to obtain α and S/L. From Equation (27) the required angle of turning of the upstream edge of the jet Φ is found for a chosen value of β. The values of h/w and g/w corresponding to this Φ are found from the graphical characteristic construction of the jet shape. The specific impulse ratio and lift coefficient are then calculated from Equations (31) and (32).

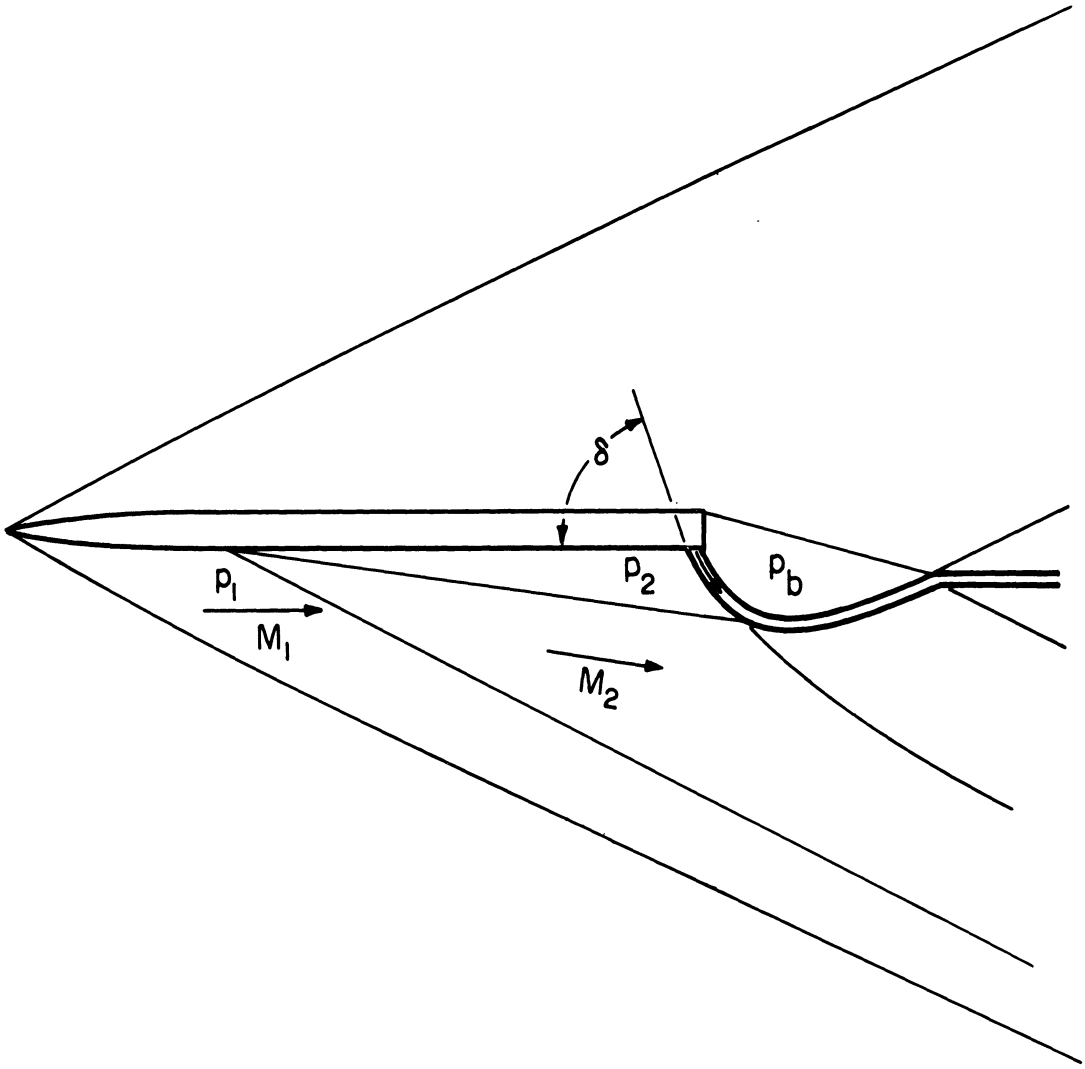

Figure 1. Supersonic airfoil with jet flap.

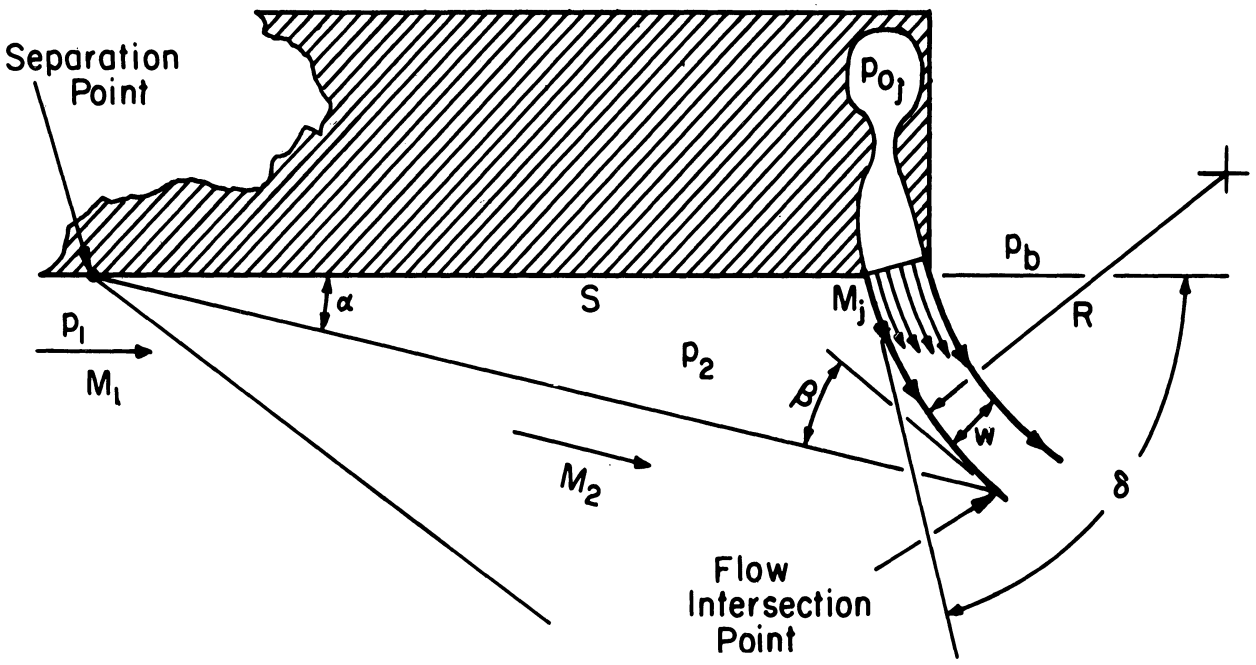

Figure 2. Two-dimensional circular-arc jet-flap model

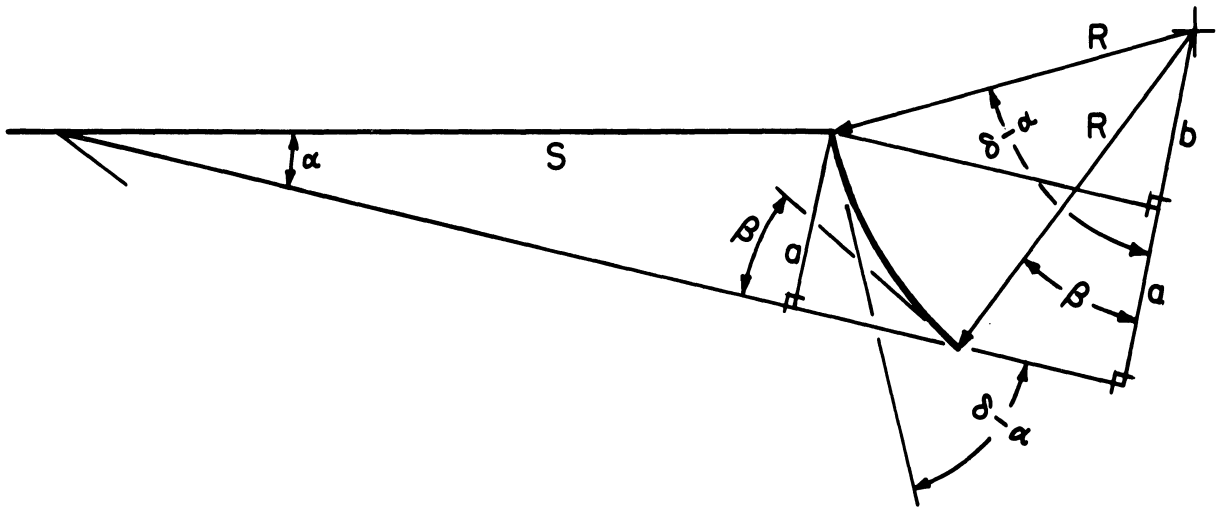

Figure 3. Geometrical relationships between the separation distance and the jet radius of curvature.

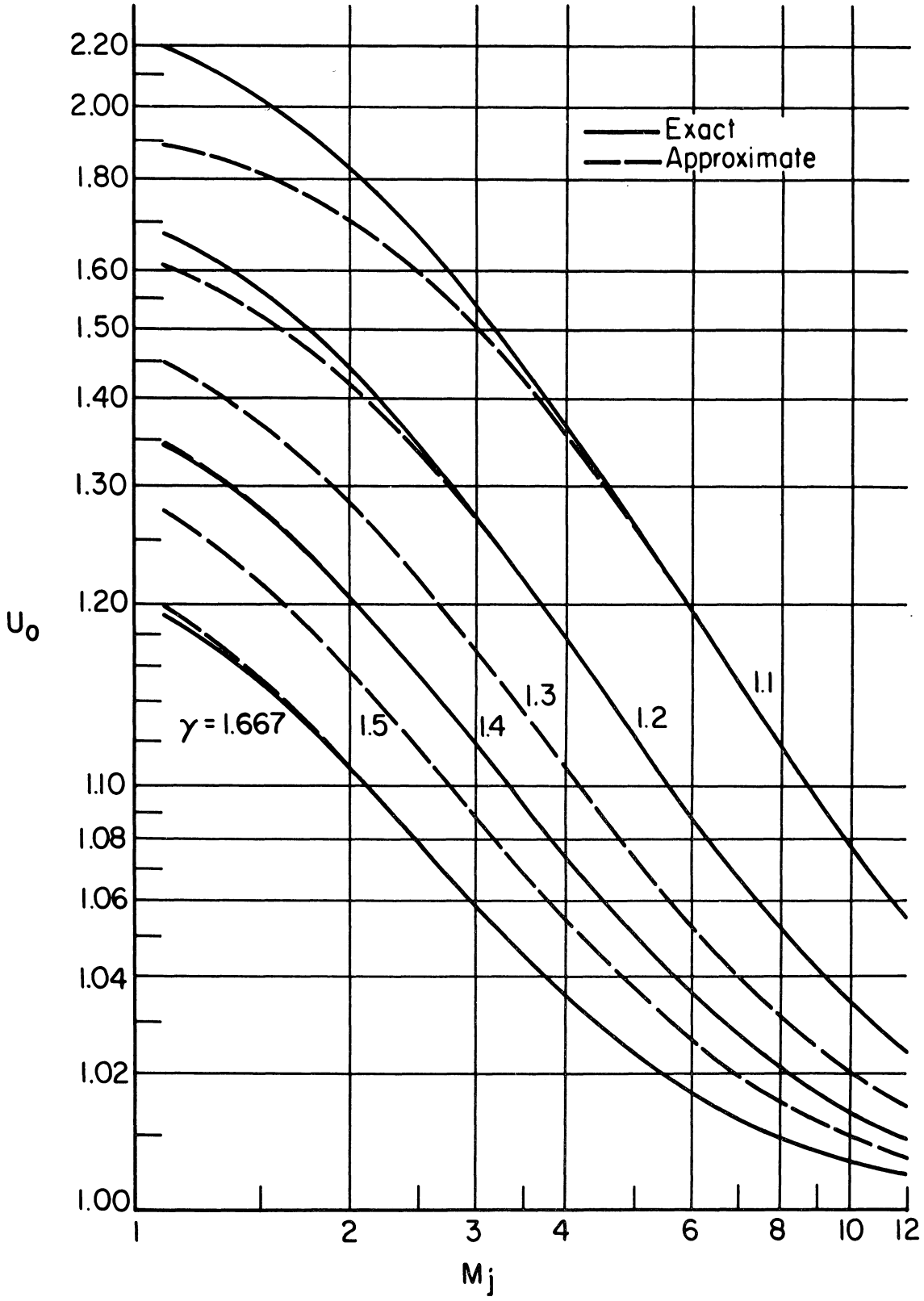

Figure 4. Variation with jet Mach number of the value of the infinite series in Equation (10) for $p_b = 0$ and various jet gas specific heat ratios.

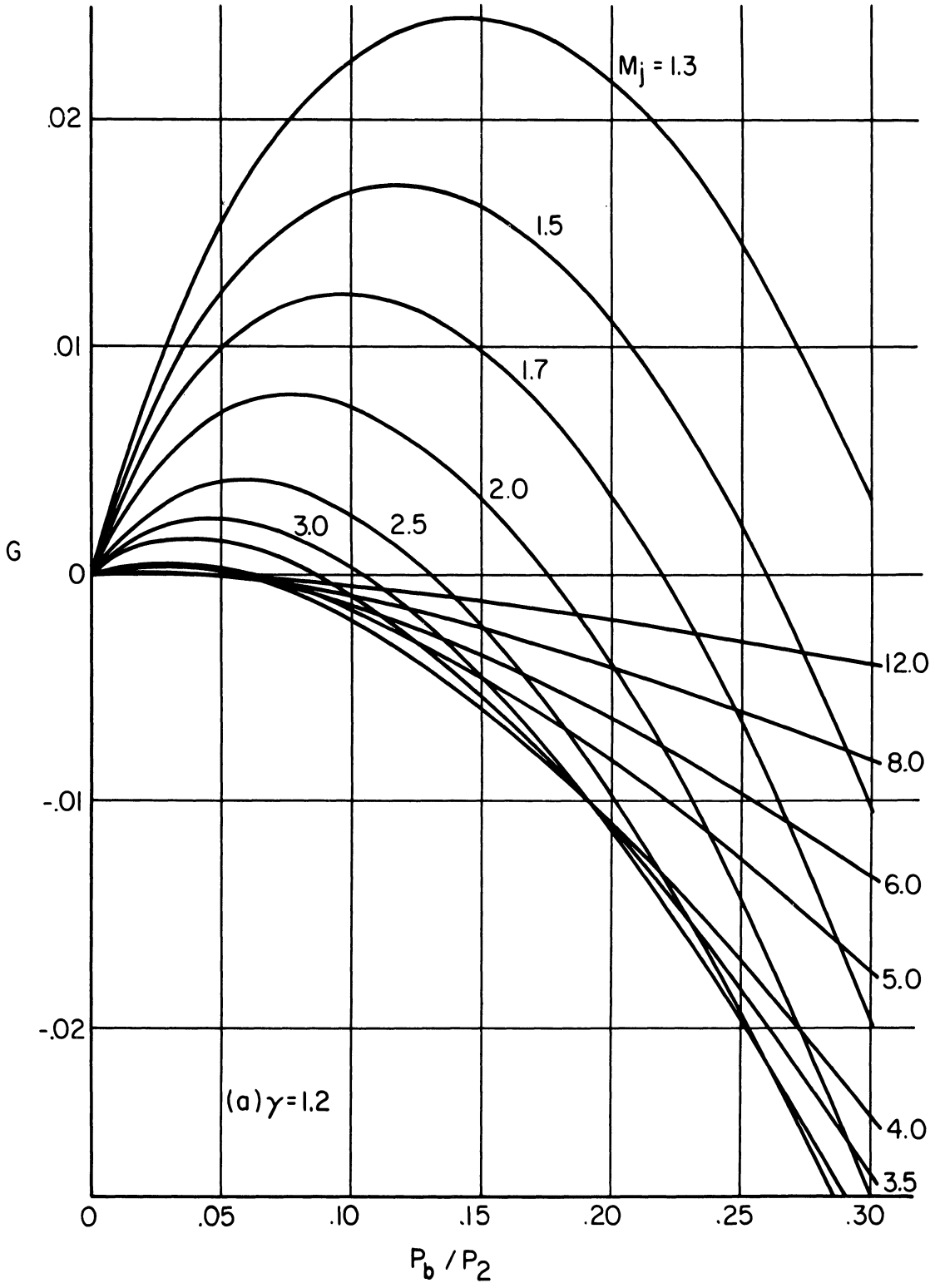

Figure 5. Variation with base pressure of the correction term in the equation $U = U_o - p_b/p_2 + G$ for various jet Mach numbers.

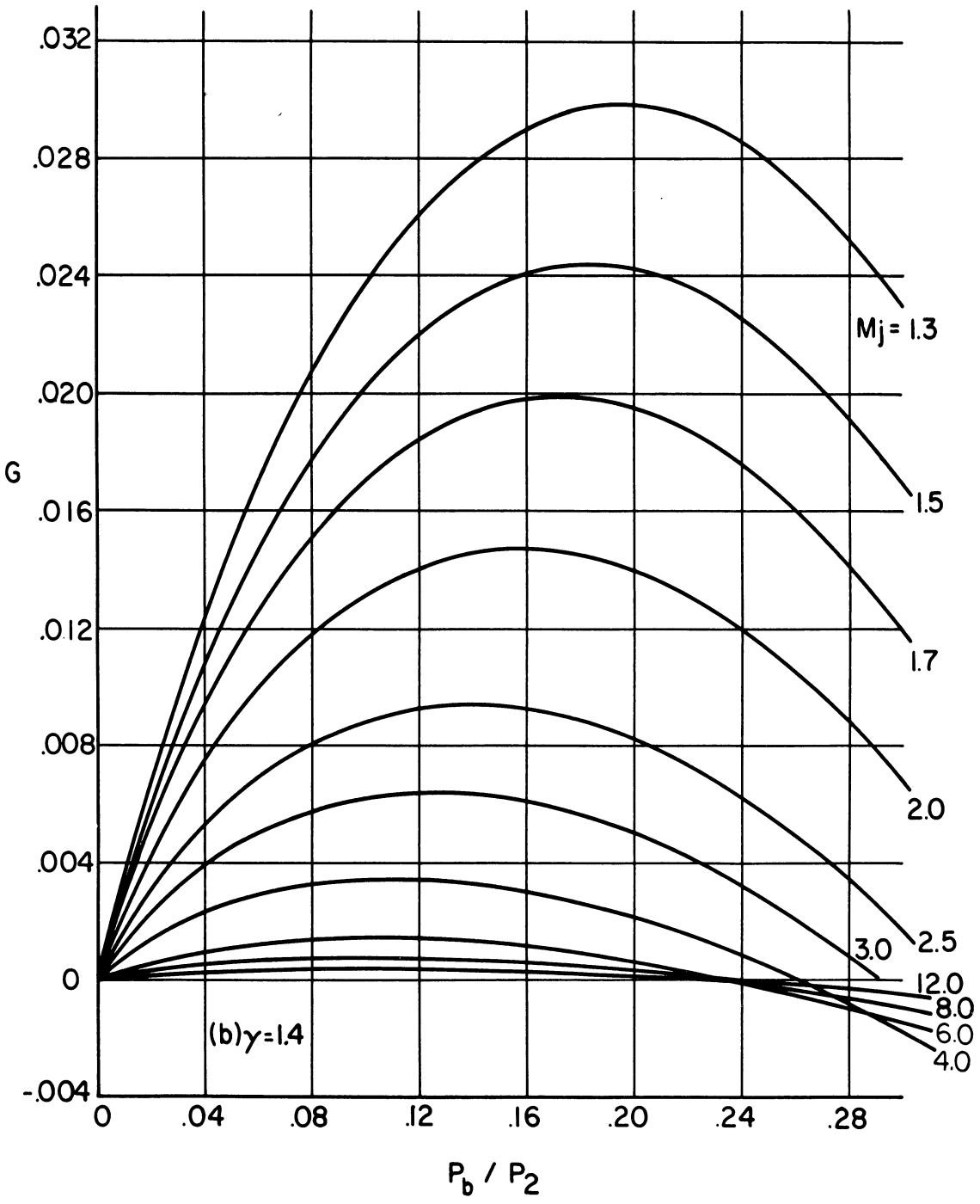

Figure 5. Continued.

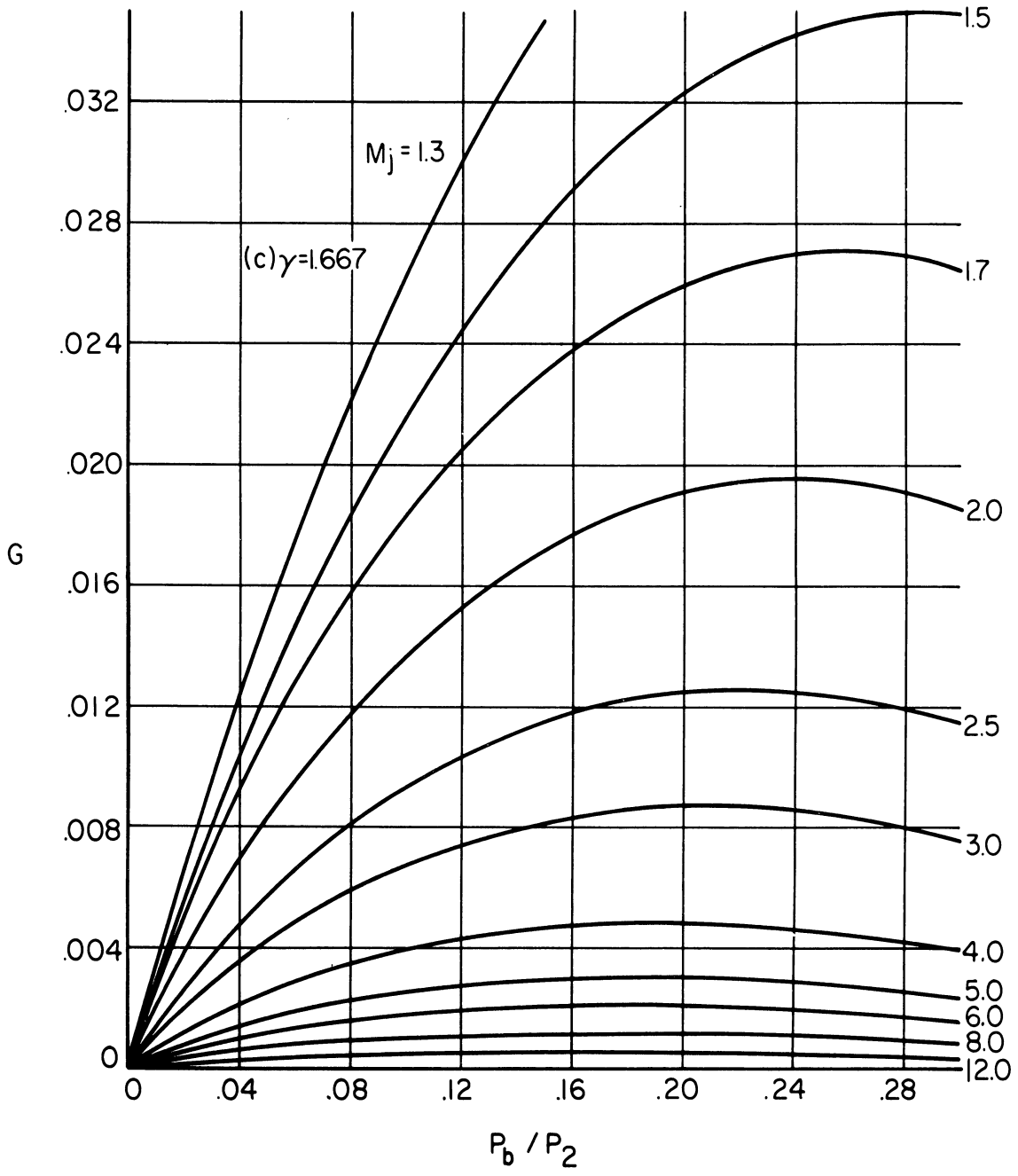

Figure 5. Concluded.

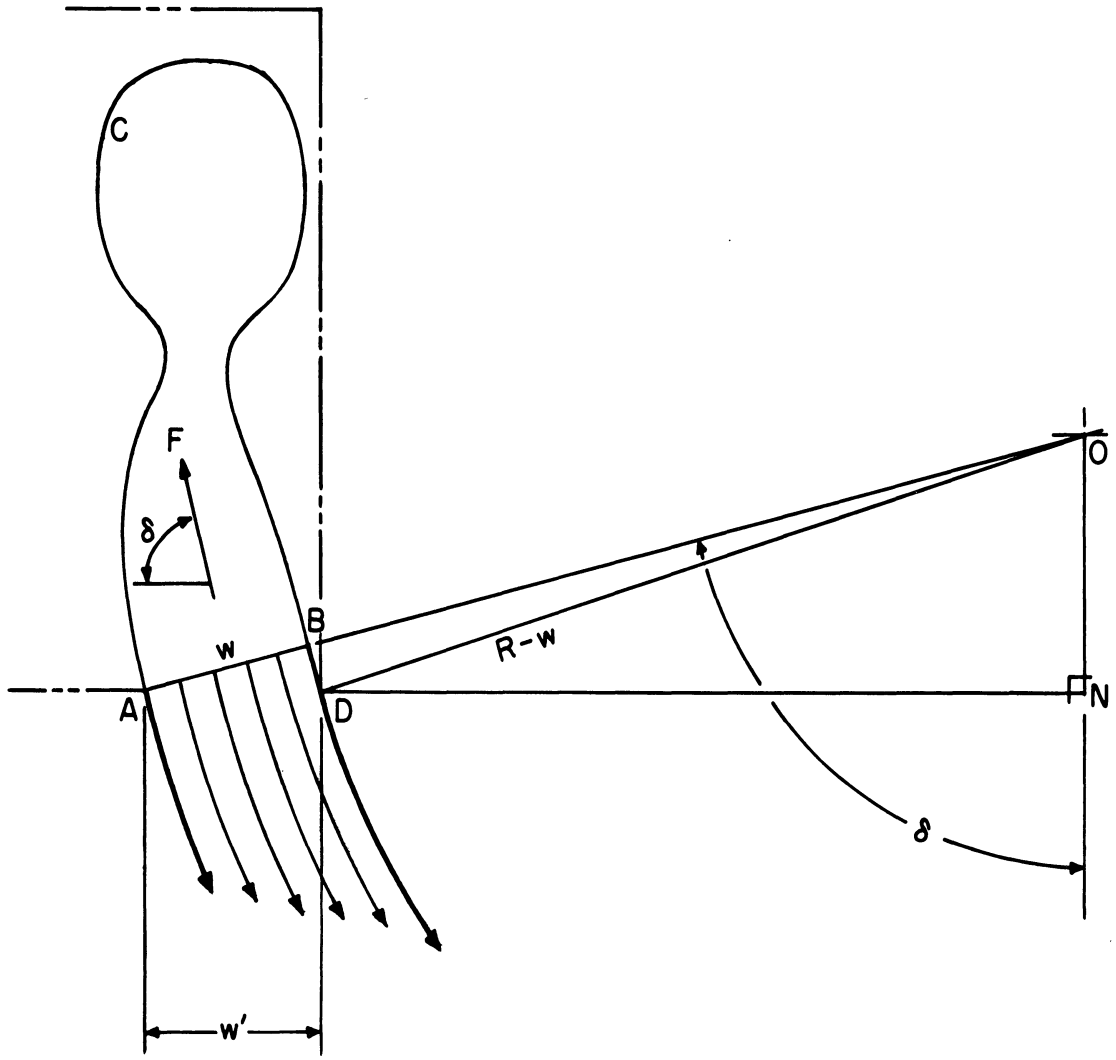

Figure 6. Geometrical relationships for determining the force components.

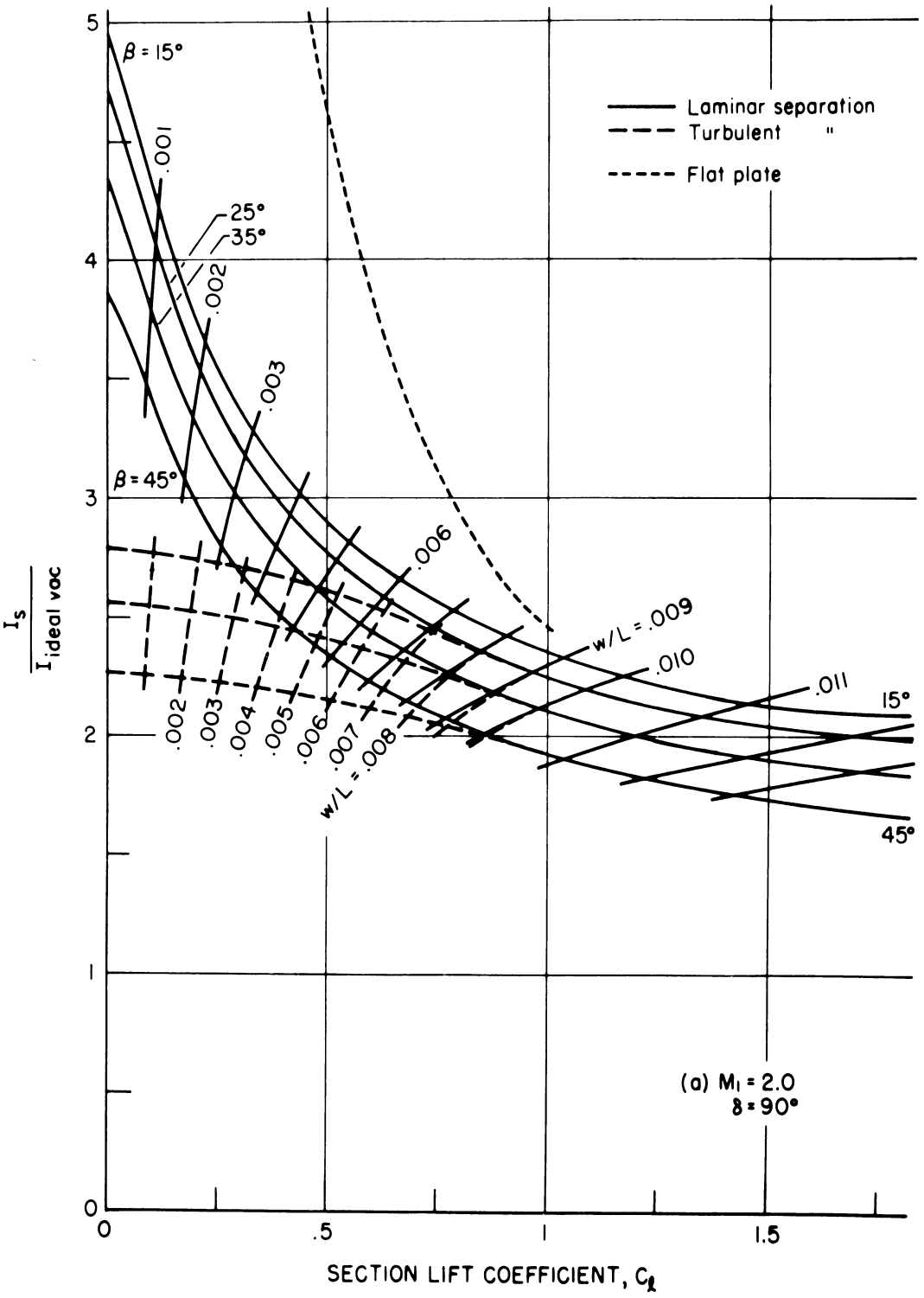

Figure 7. Specific impulse vs. section lift coefficient for various flow intersection angles and jet widths. $M_j = 8.0$, $\gamma = 1.4$, $(p_{0j}/p_2 = 9763)$, $p_b/p_1 = .3$, $Re_L = 10^7$.

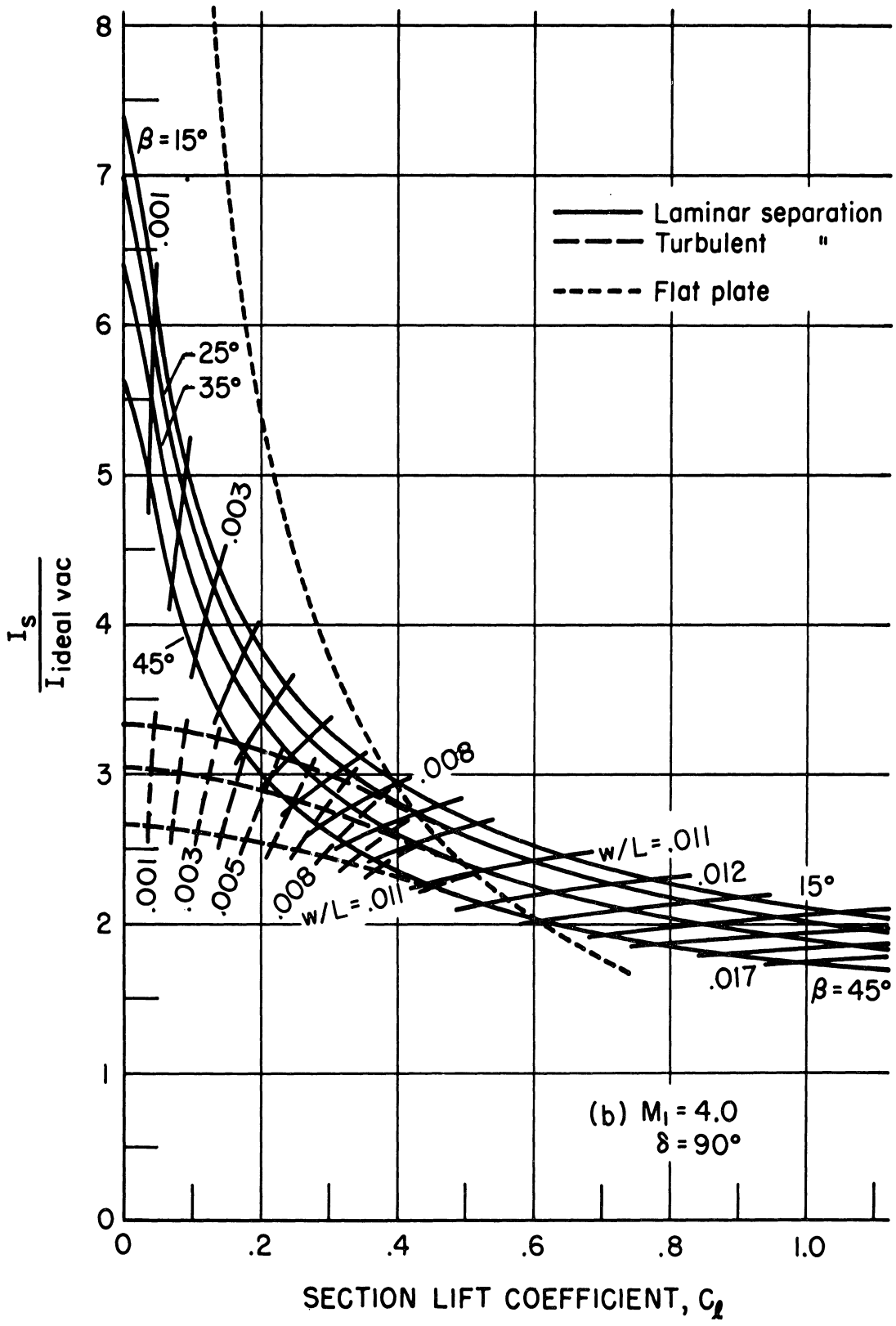

Figure 7. Continued.

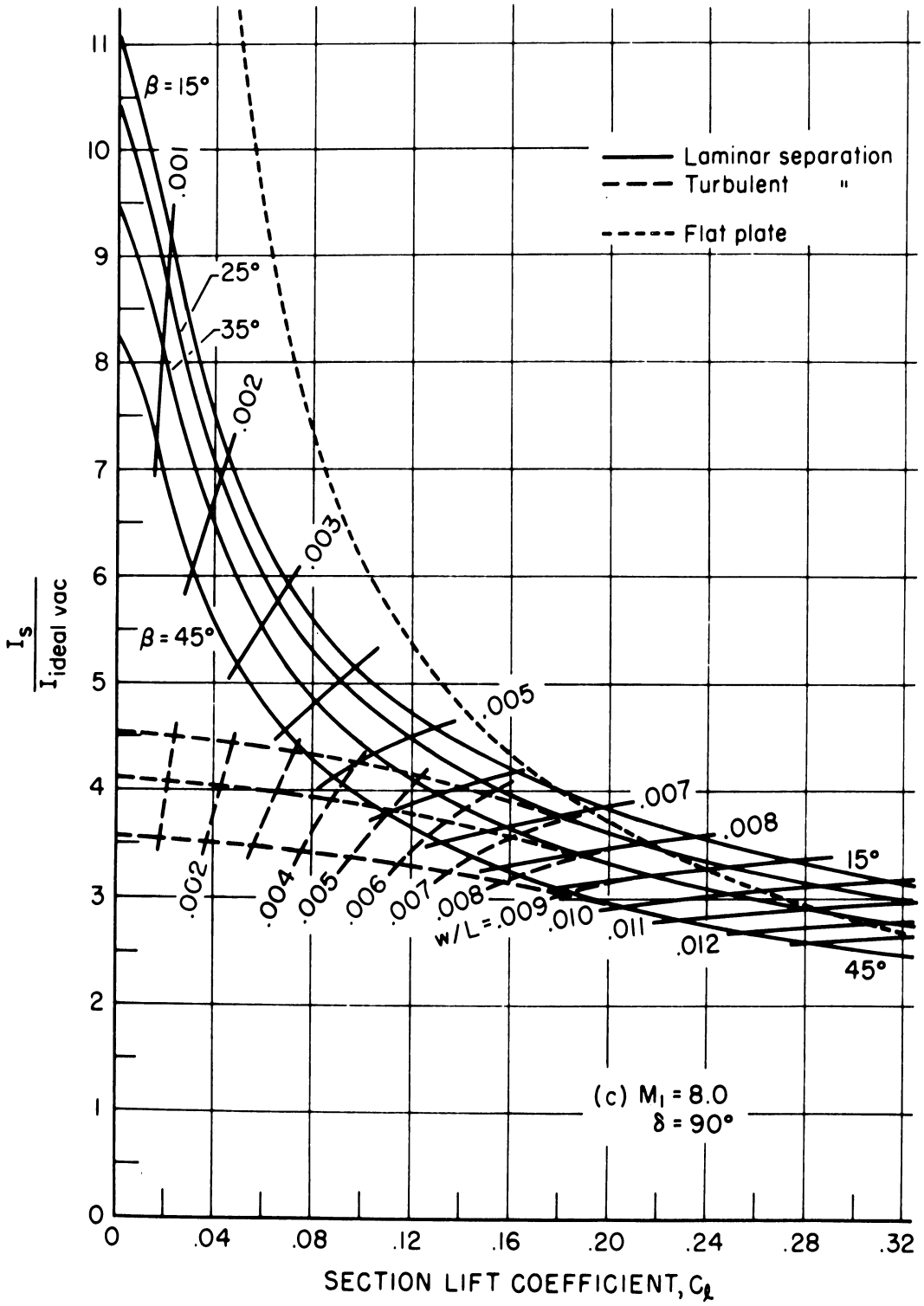

Figure 7. Continued.

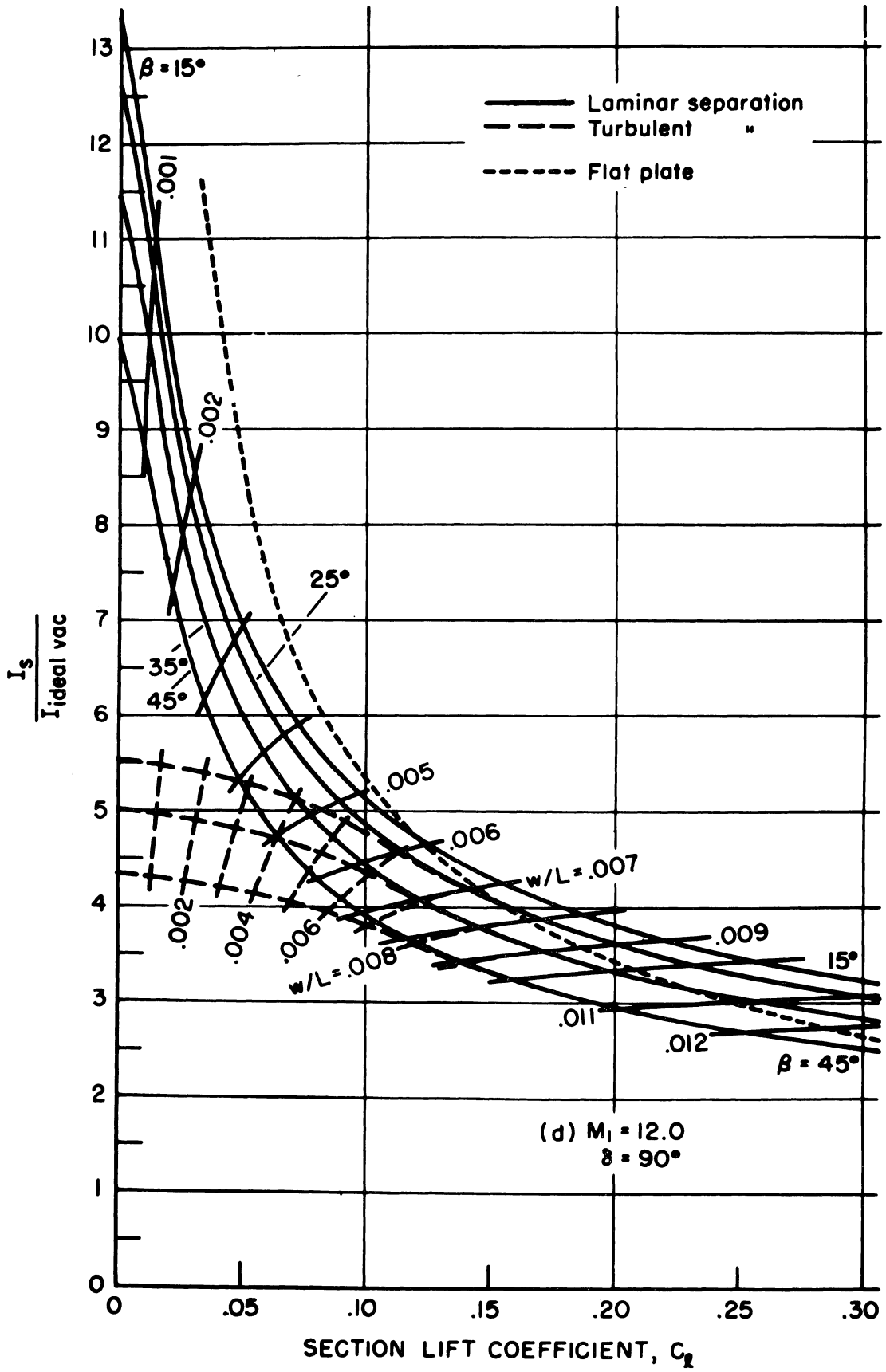

Figure 7. Continued.

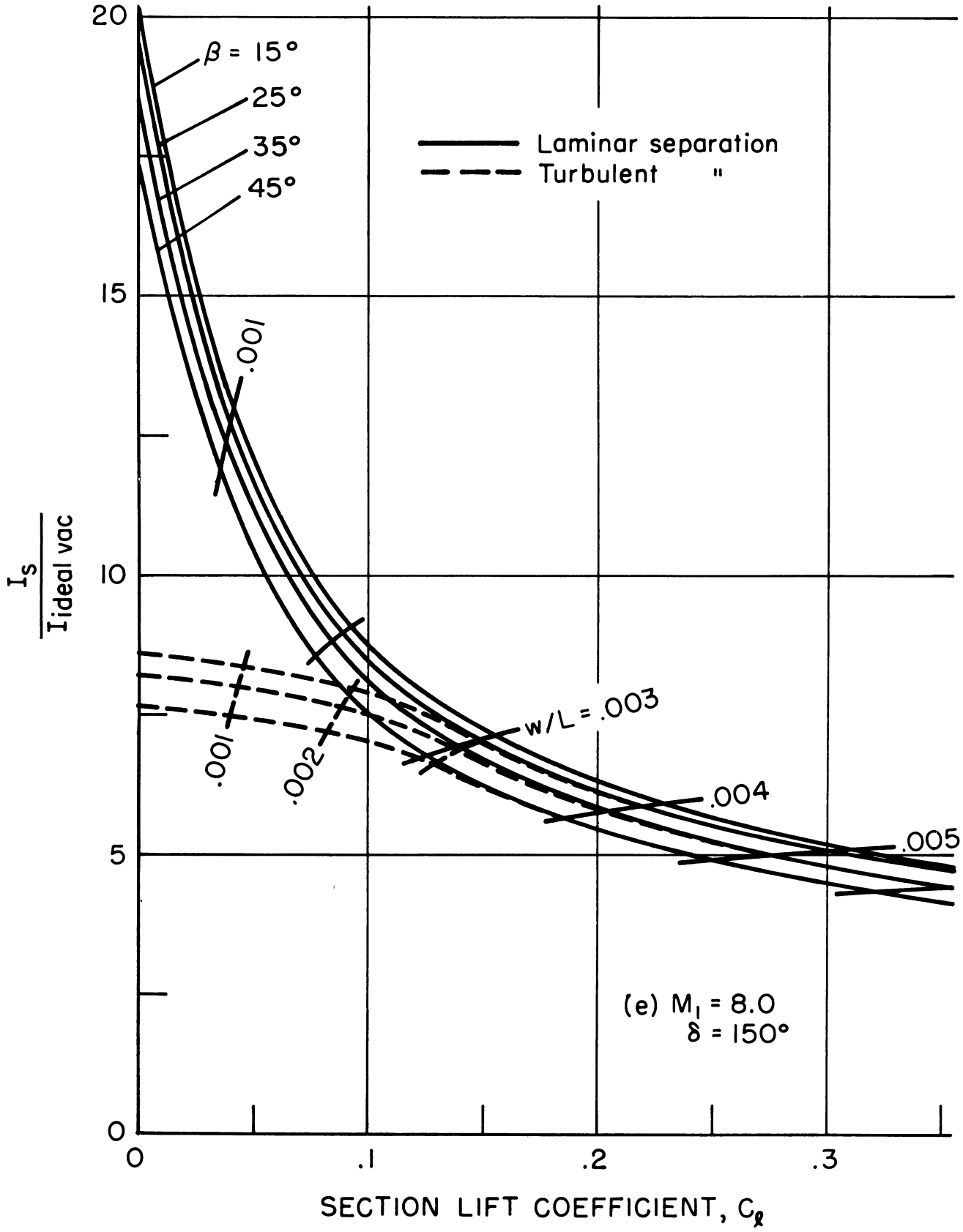

Figure 7. Concluded.

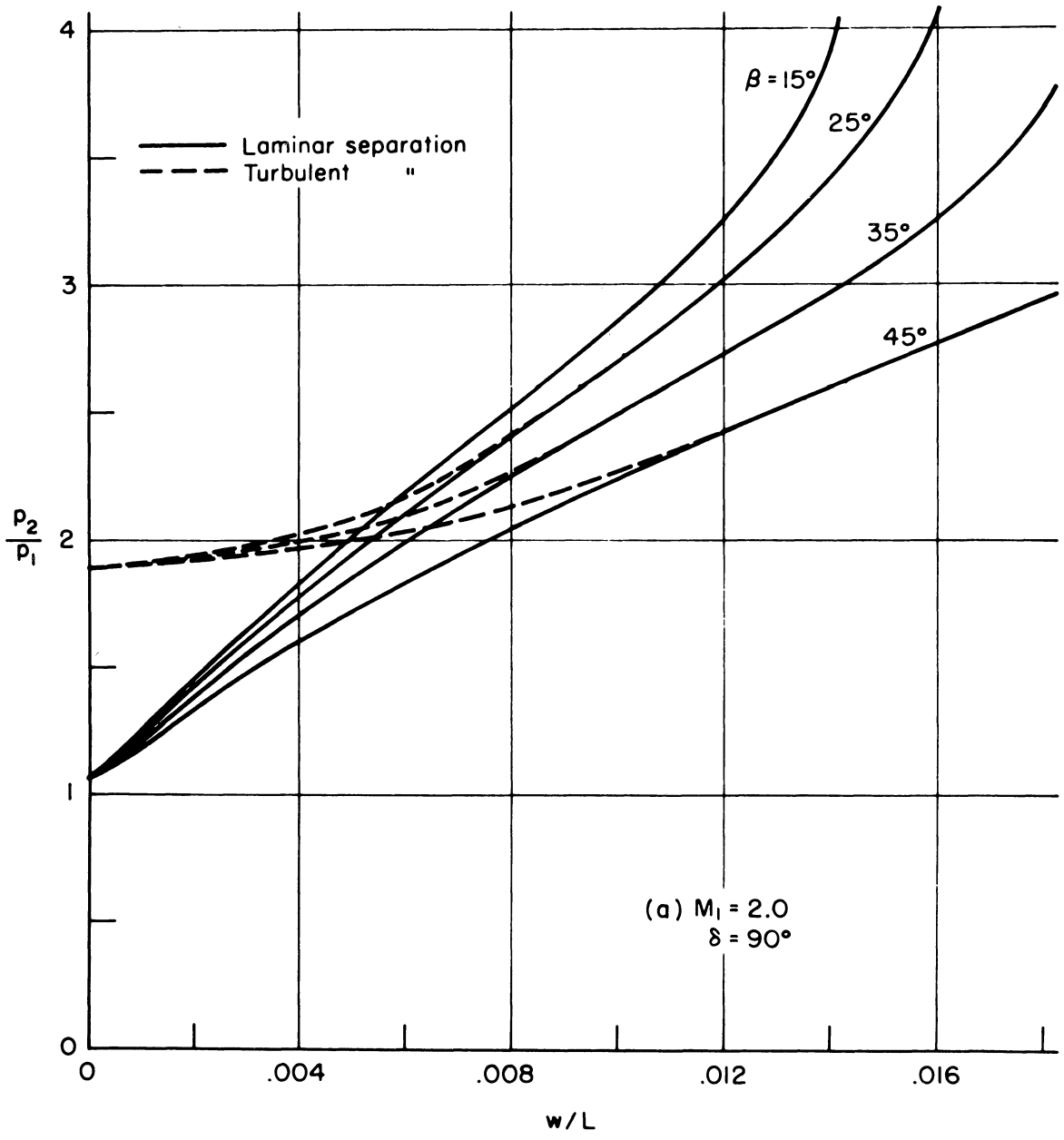

Figure 8. Plateau pressure rise vs. jet width for various flow intersection angles. $M_j = 8.0$, $\gamma = 1.4$, $p_b/p_1 = .3$, $Re_L = 10^7$.

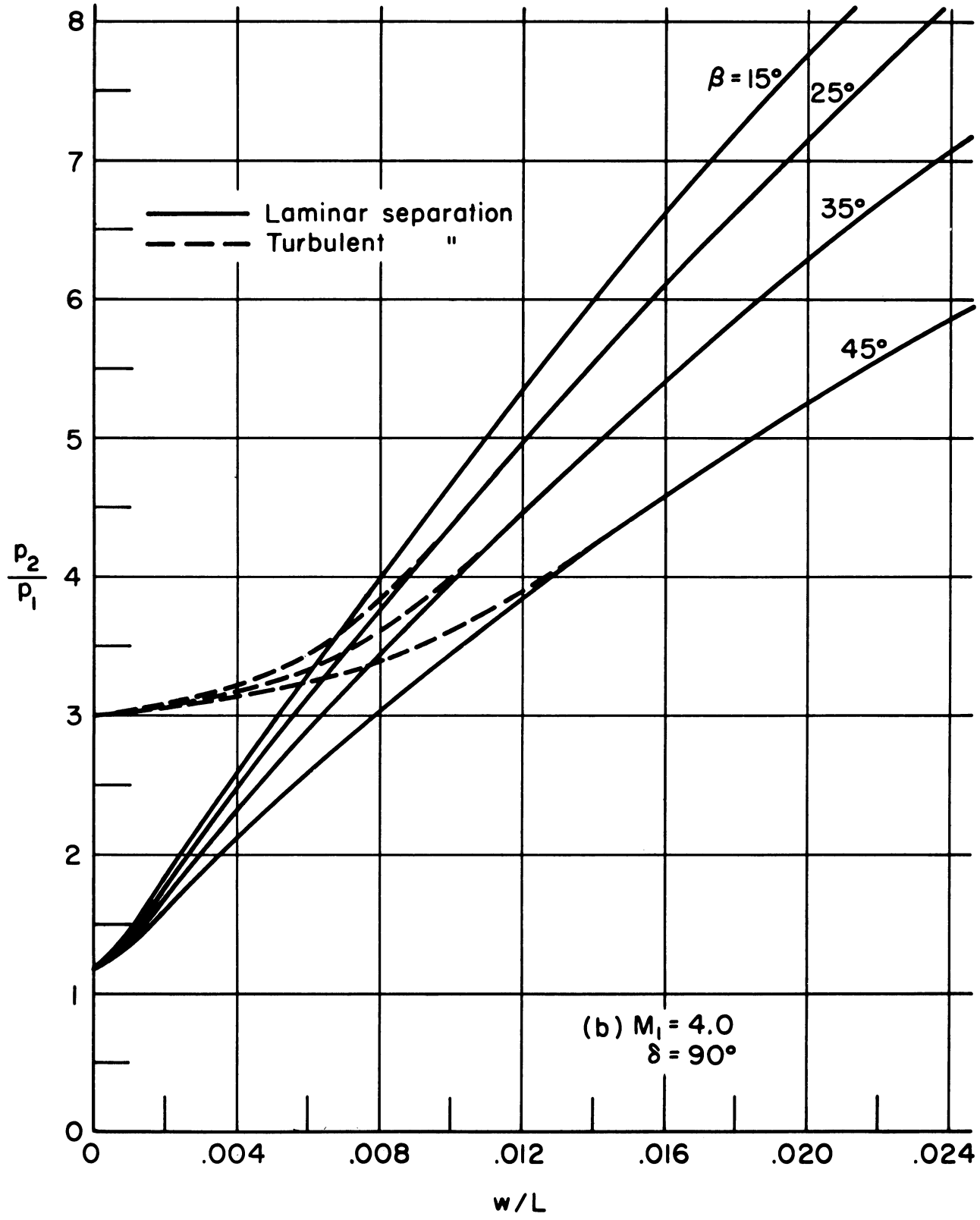

Figure 8. Continued.

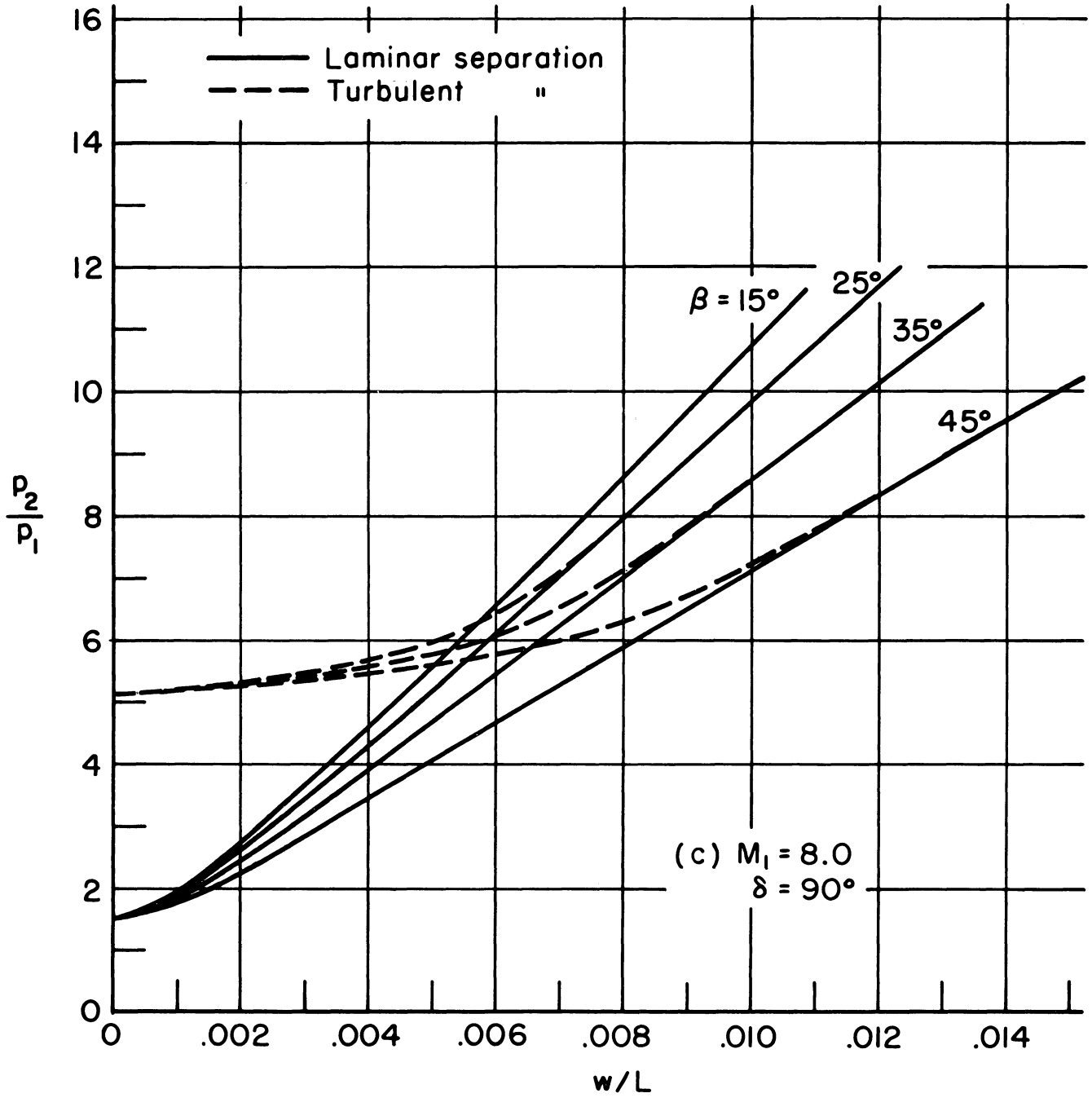

Figure 8. Continued.

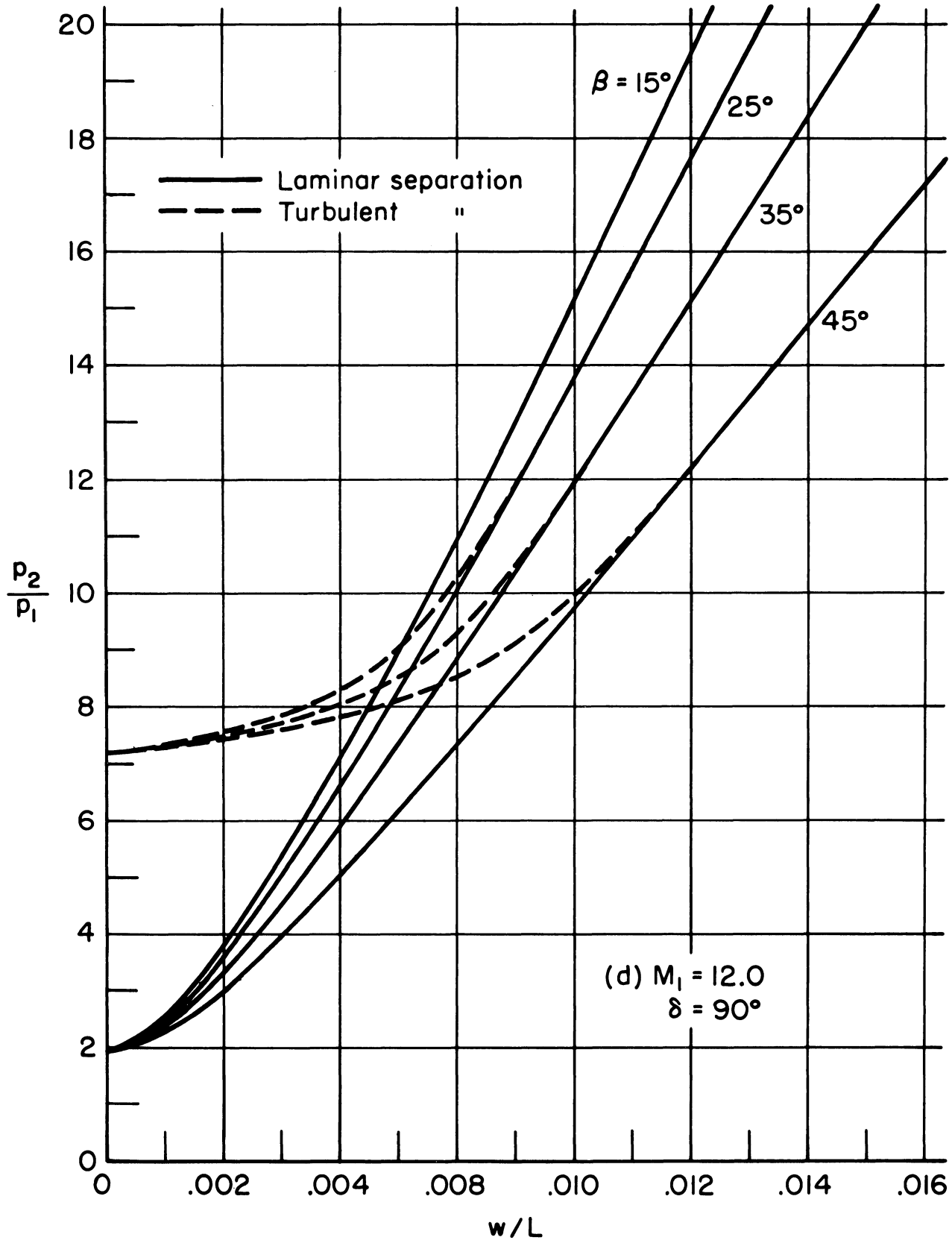

Figure 8. Continued.

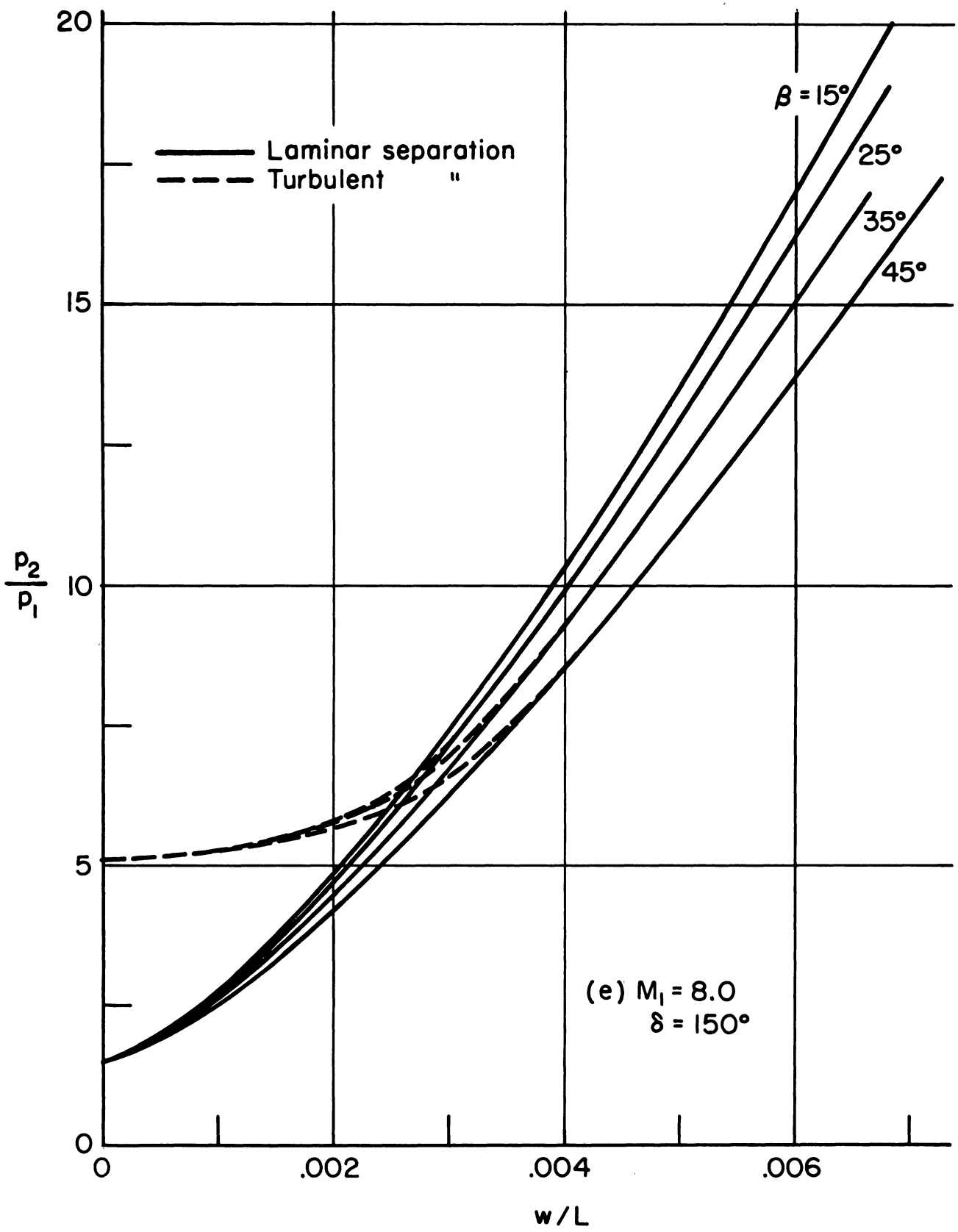

Figure 8. Concluded.

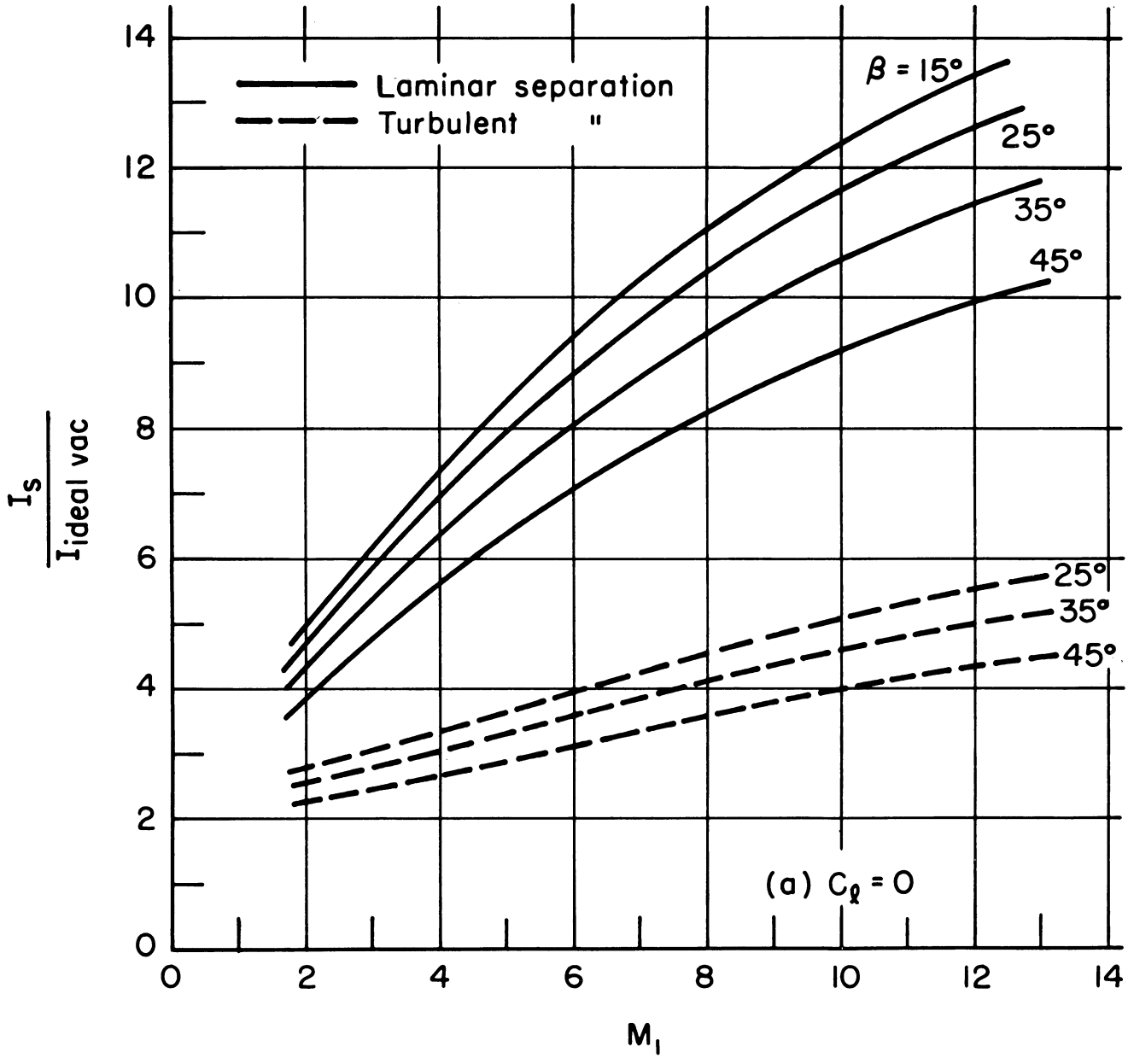

Figure 9. Specific impulse vs. free-stream Mach number for $\delta = 90°$. $M_j = 8.0$, $\gamma = 1.4$, $p_b/p_1 = .3$, $Re_L = 10^7$.

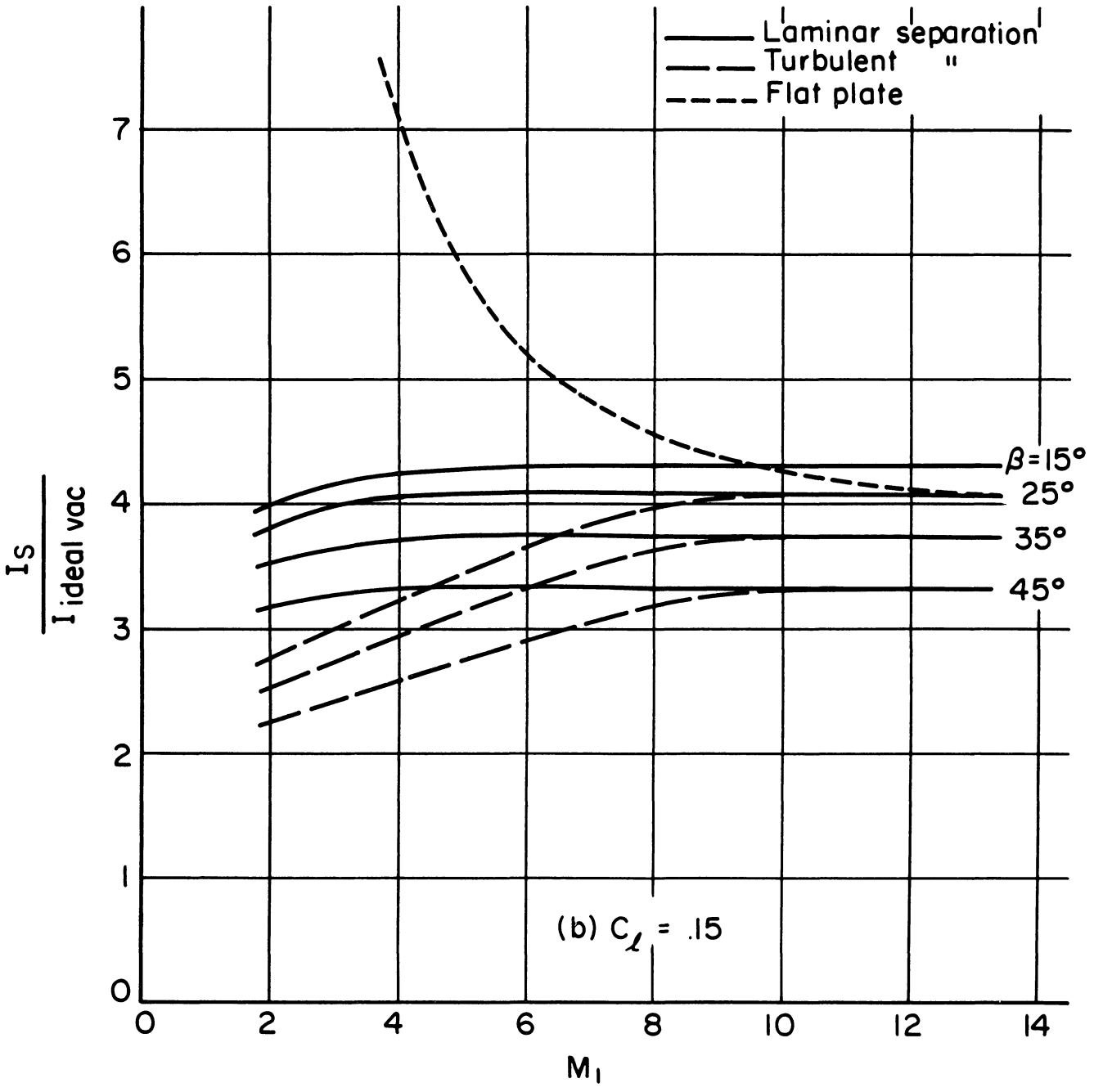

Figure 9. Concluded.

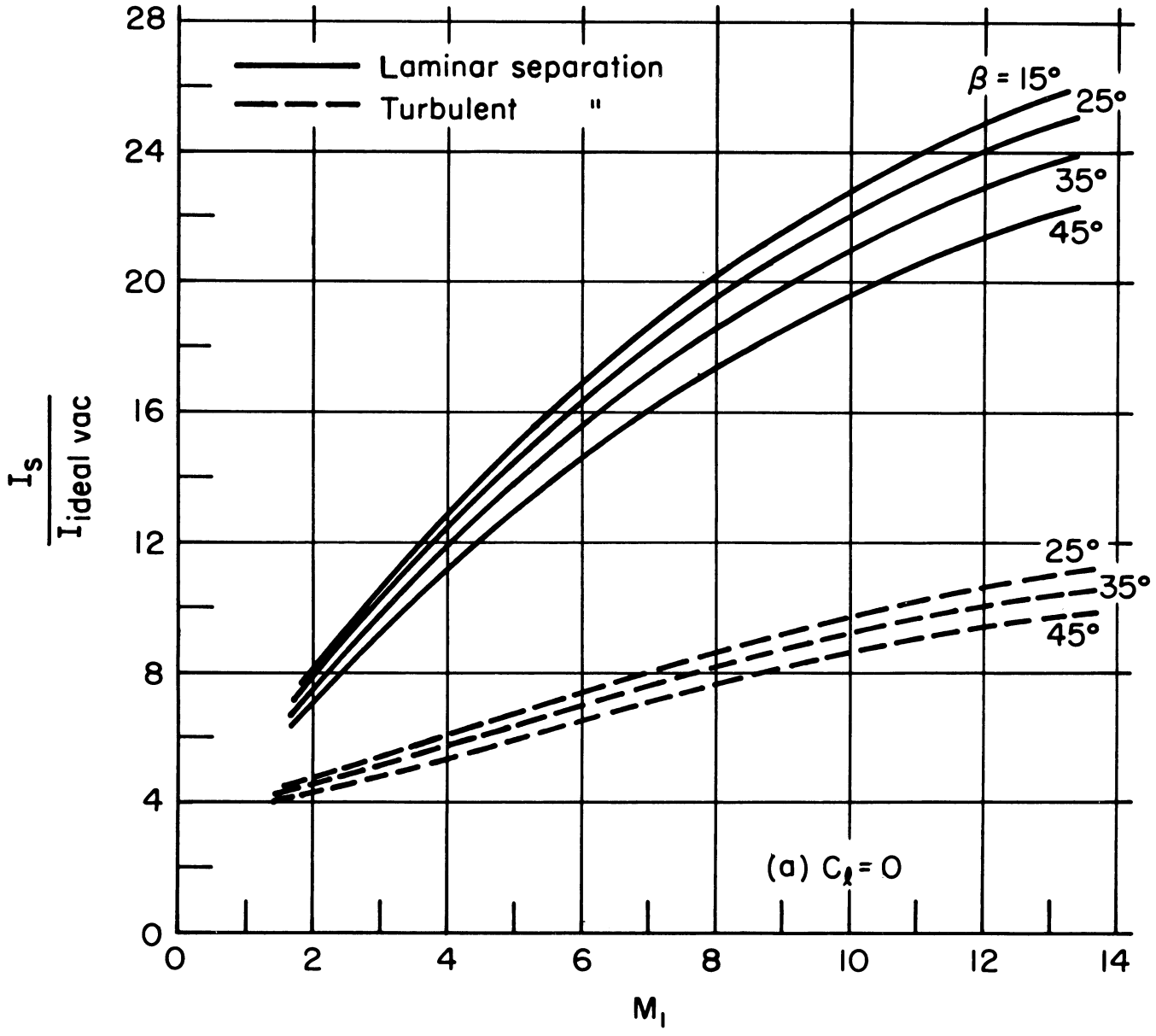

Figure 10. Specific impulse vs. free-stream Mach number for $\delta = 150°$. $M_j = 8.0$, $\gamma = 1.4$, $p_b/p_1 = .3$, $Re_L = 10^7$.

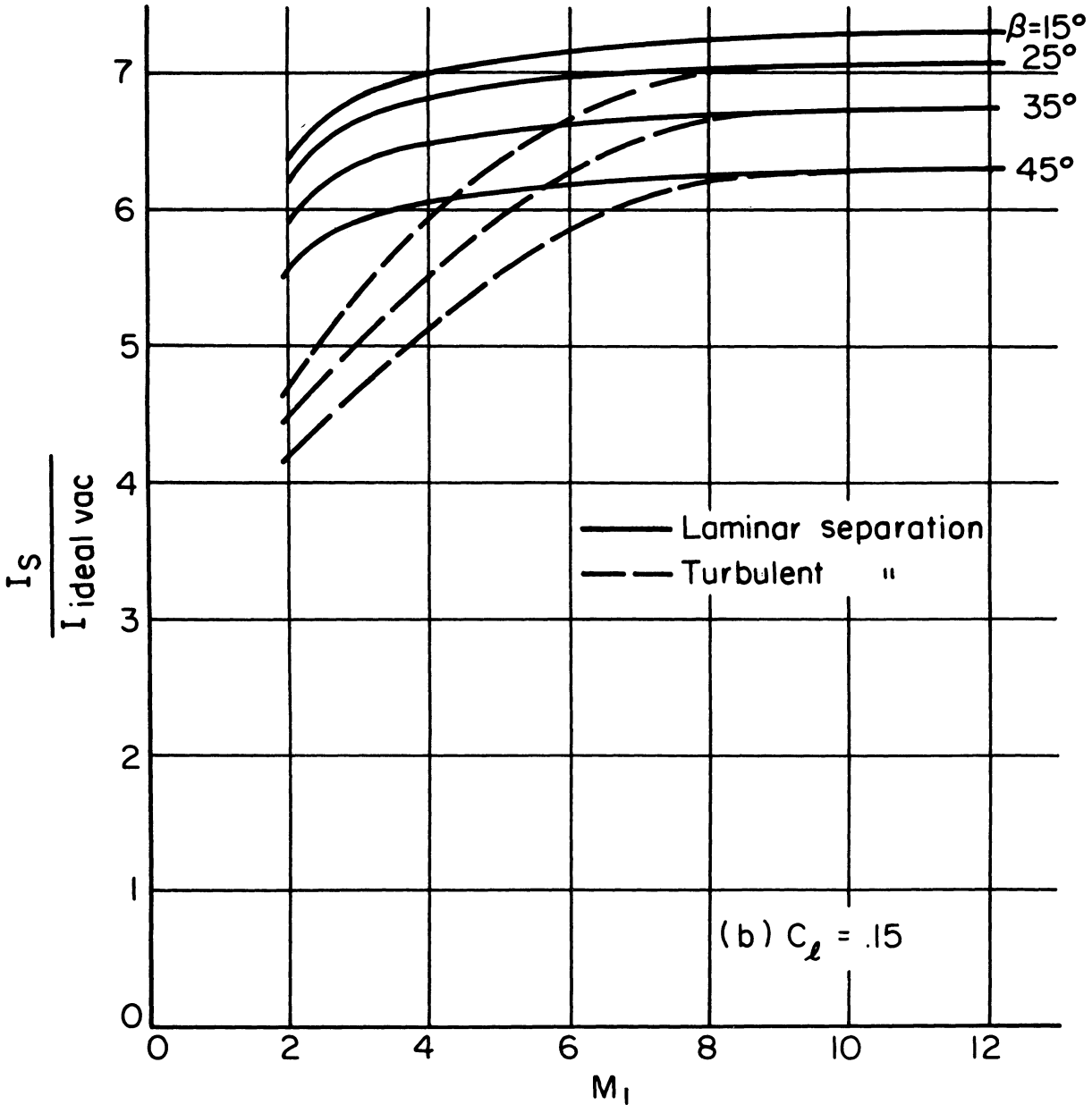

Figure 10. Concluded.

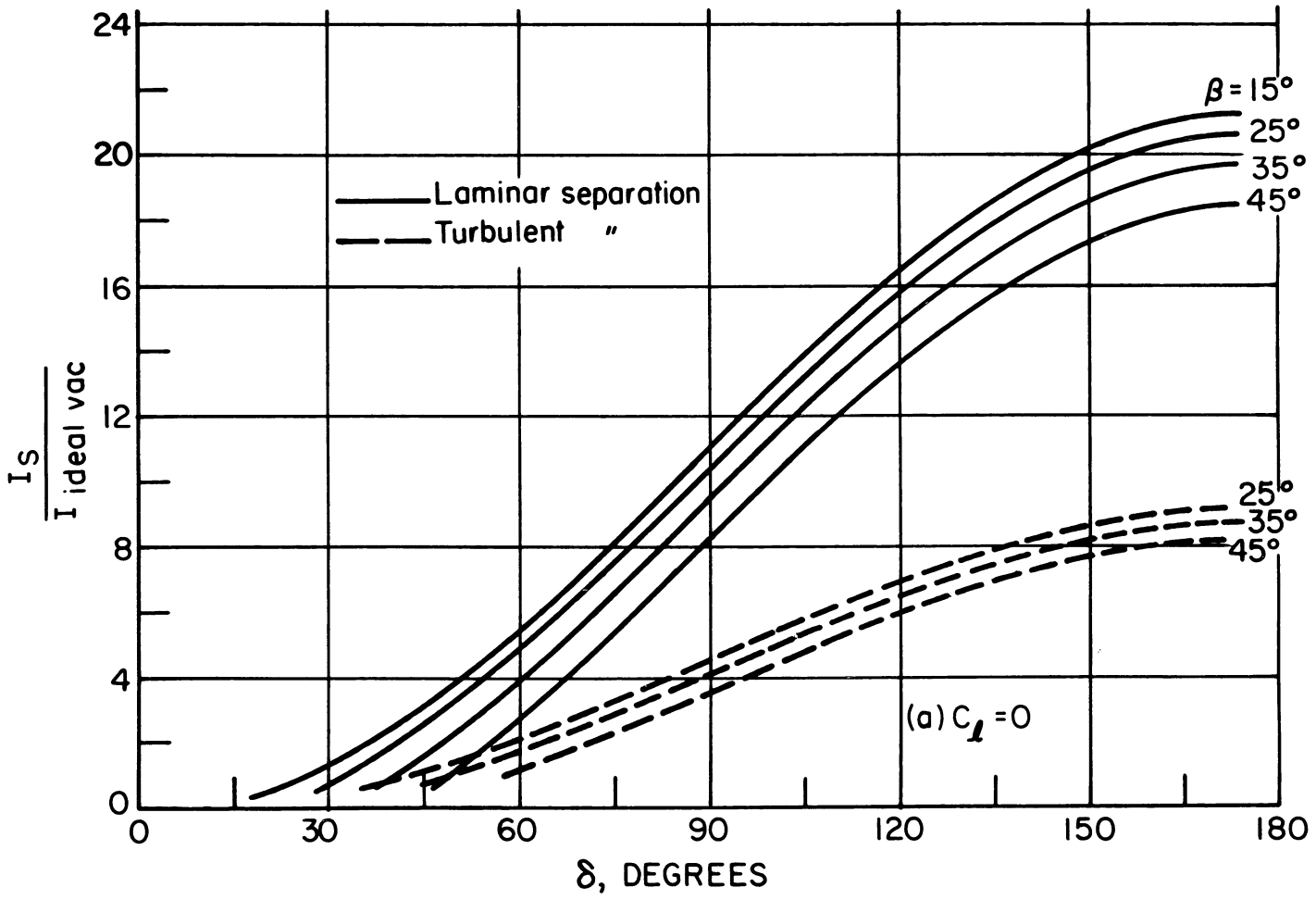

Figure 11. Specific impulse vs. jet-flap deflection angle for $M_1 = 8.0$. $M_j = 8.0$, $\gamma = 1.4$, $p_b/p_1 = .3$, $Re_L = 10^7$.

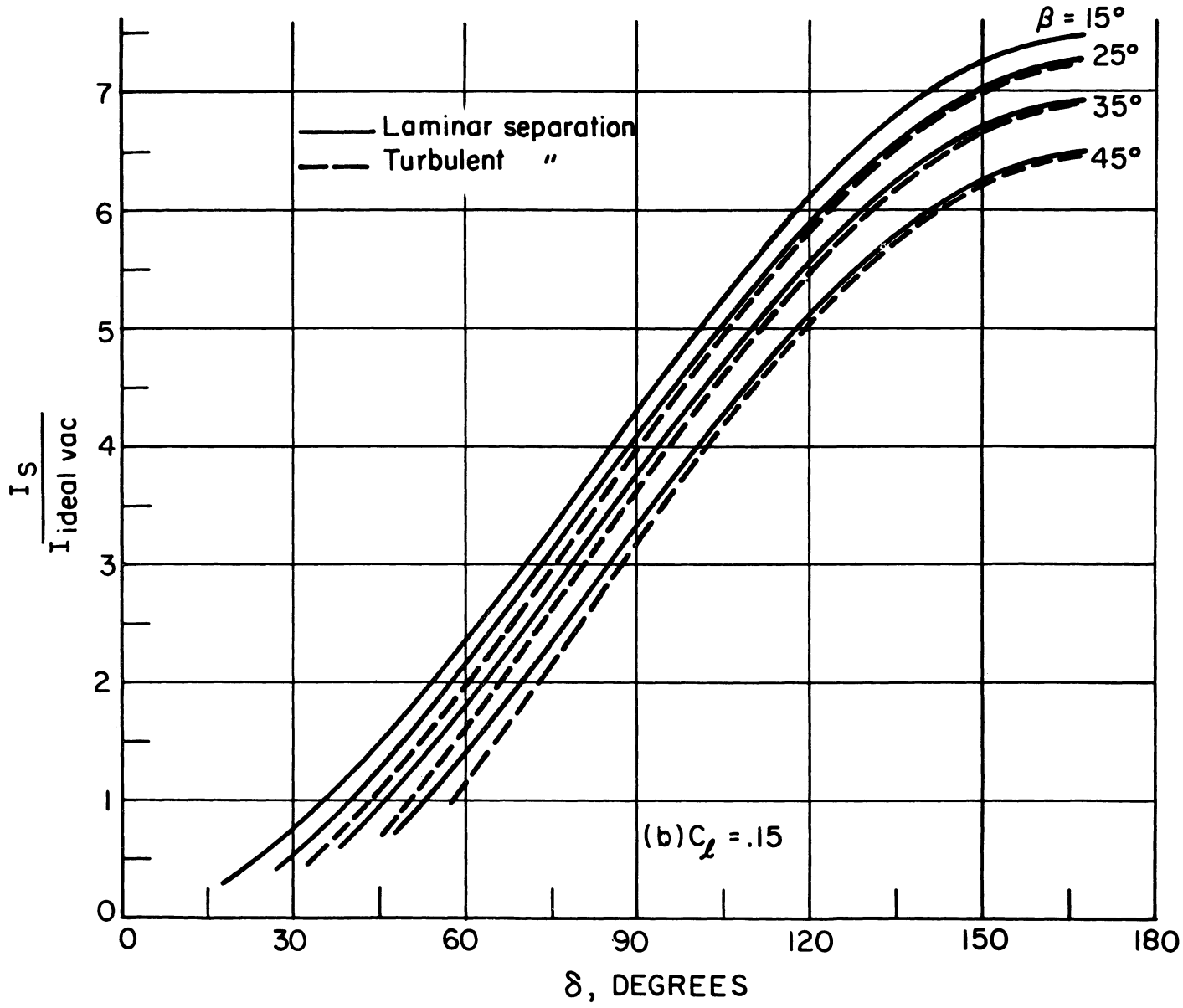

Figure 11. Concluded.

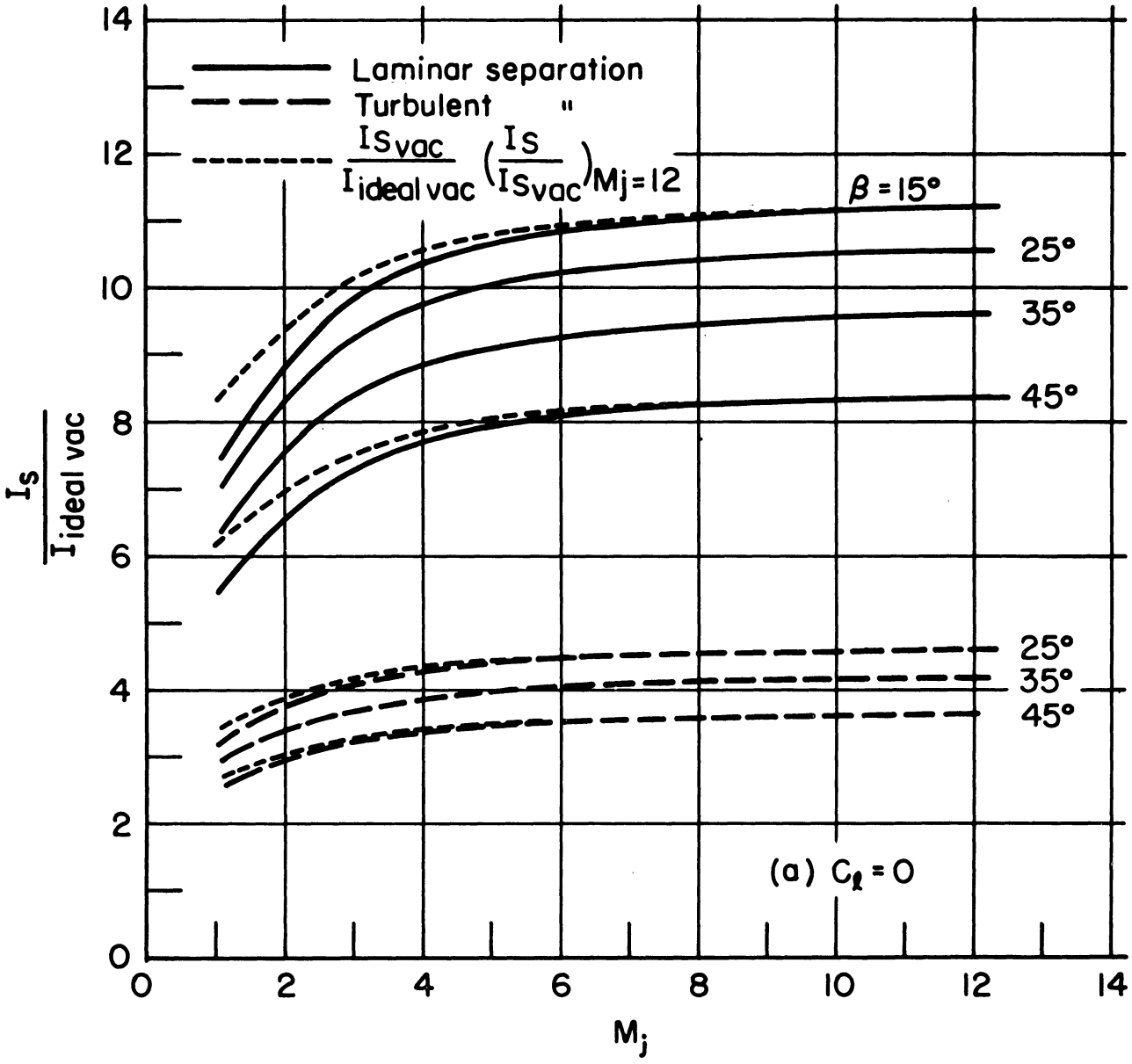

Figure 12. Specific impulse vs. jet Mach number for $M_1 = 8.0$ and $\delta = 90°$. $\gamma = 1.4$, $p_b/p_1 = .3$, $Re_L = 10^7$.

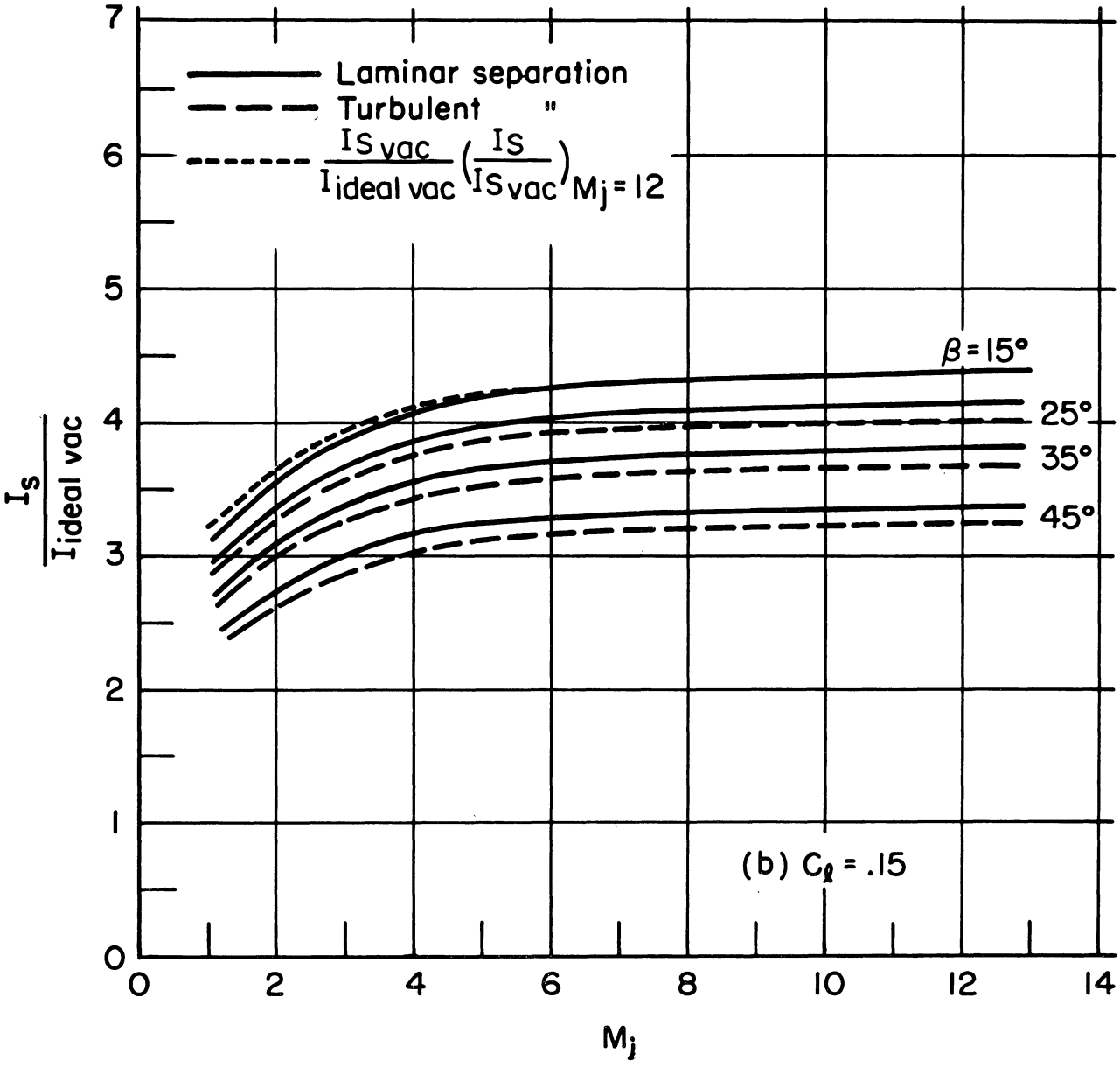

Figure 12. Concluded.

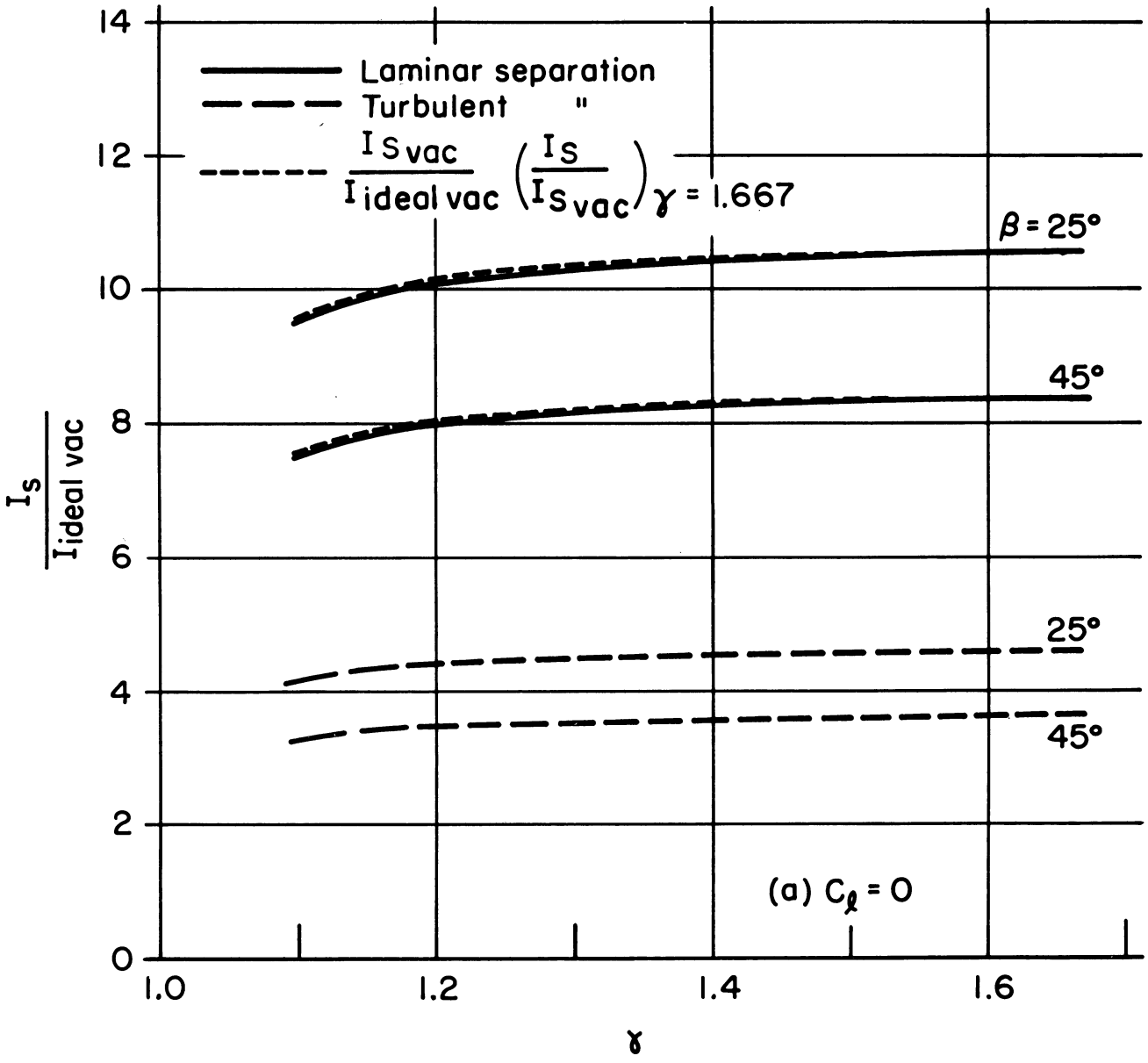

Figure 13. Specific impulse vs. jet gas specific heat ratio for $M_1 = 8.0$ and $\delta = 90°$. $M_j = 8.0$, $p_b/p_1 = .3$, $Re_L = 10^7$.

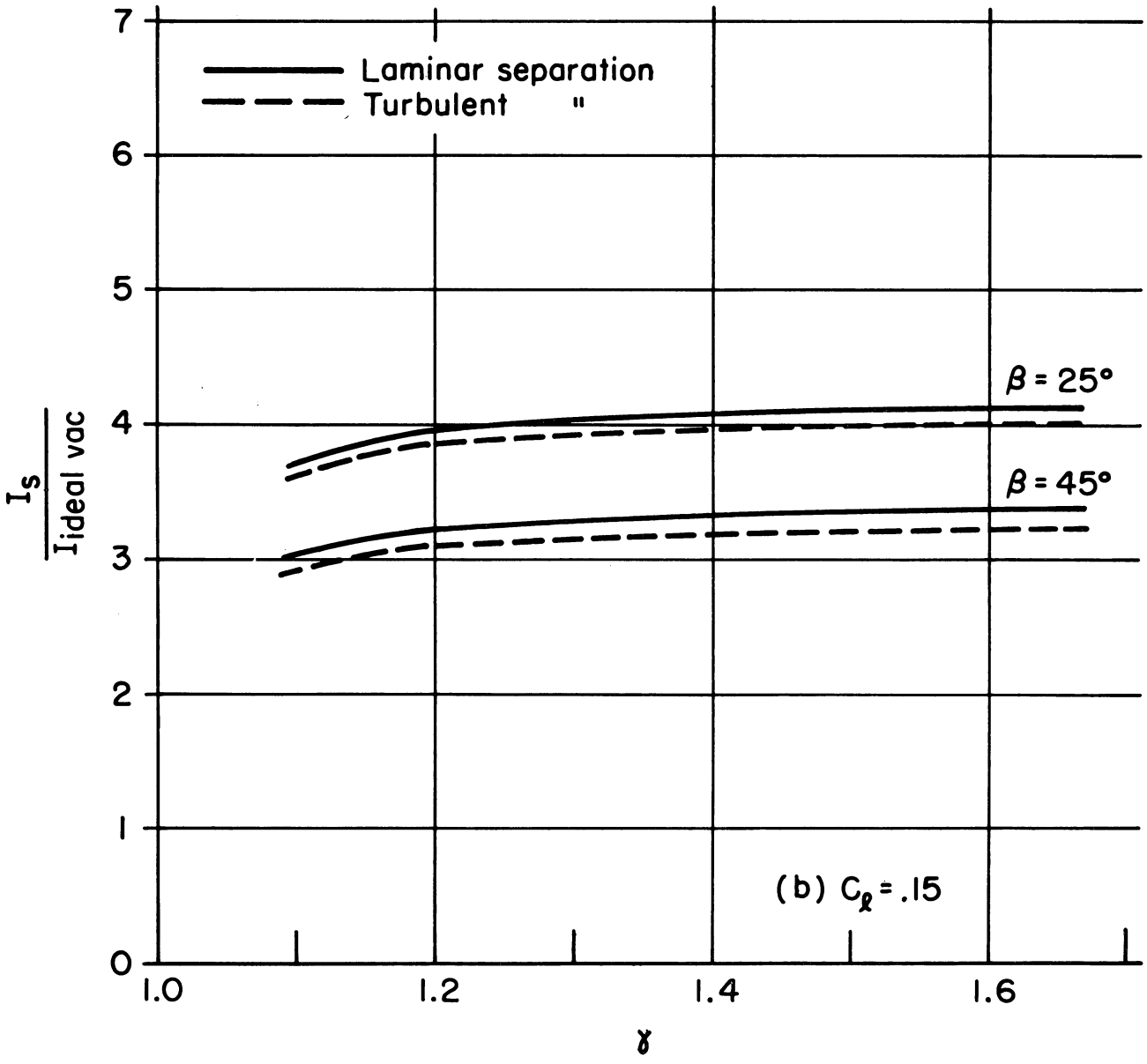

Figure 13. Concluded.

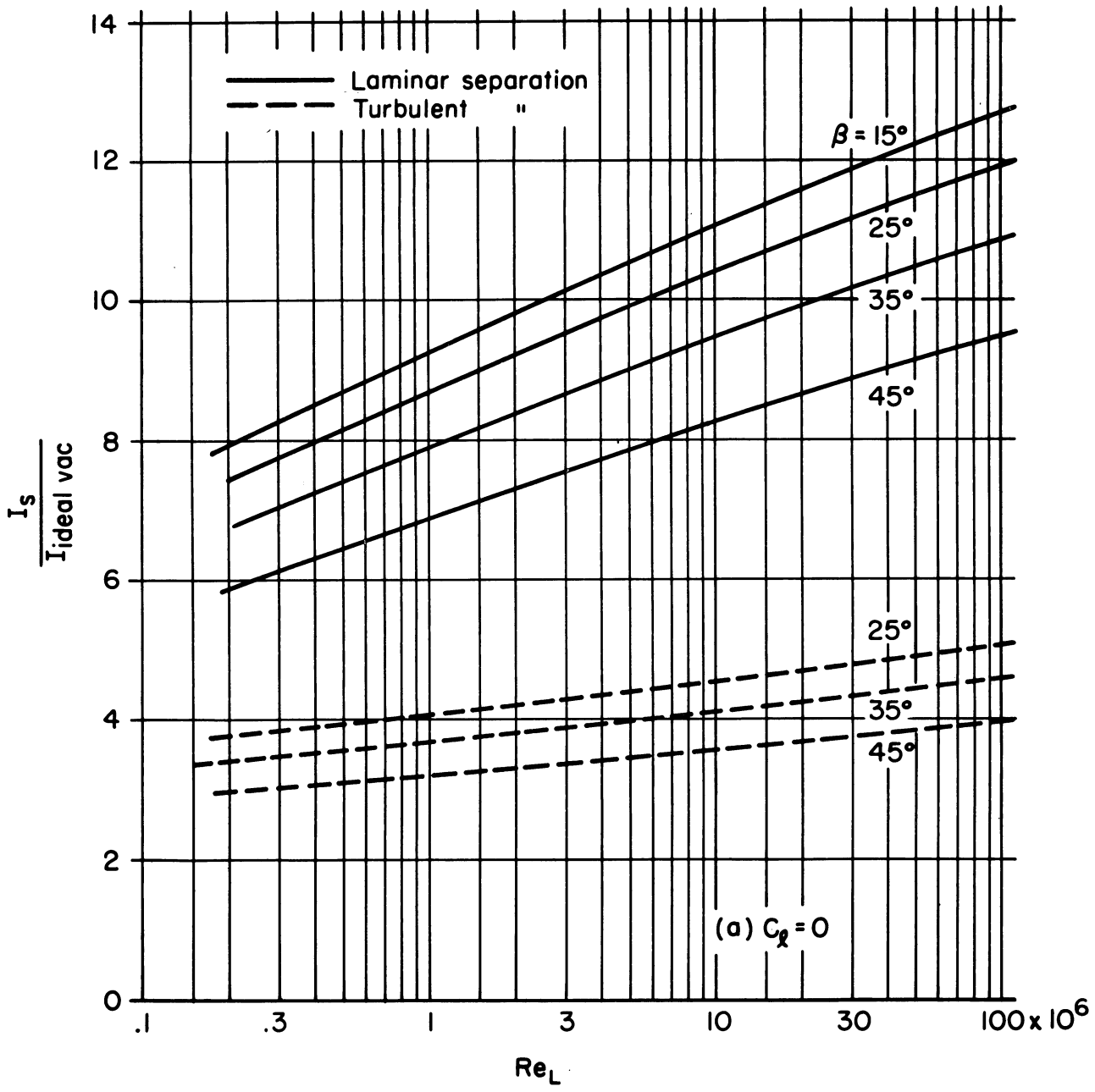

Figure 14. Specific impulse vs. Reynolds number for $M_1 = 8.0$ and $\delta = 90°$. $M_j = 8.0$, $\gamma = 1.4$, $p_b/p_1 = .3$.

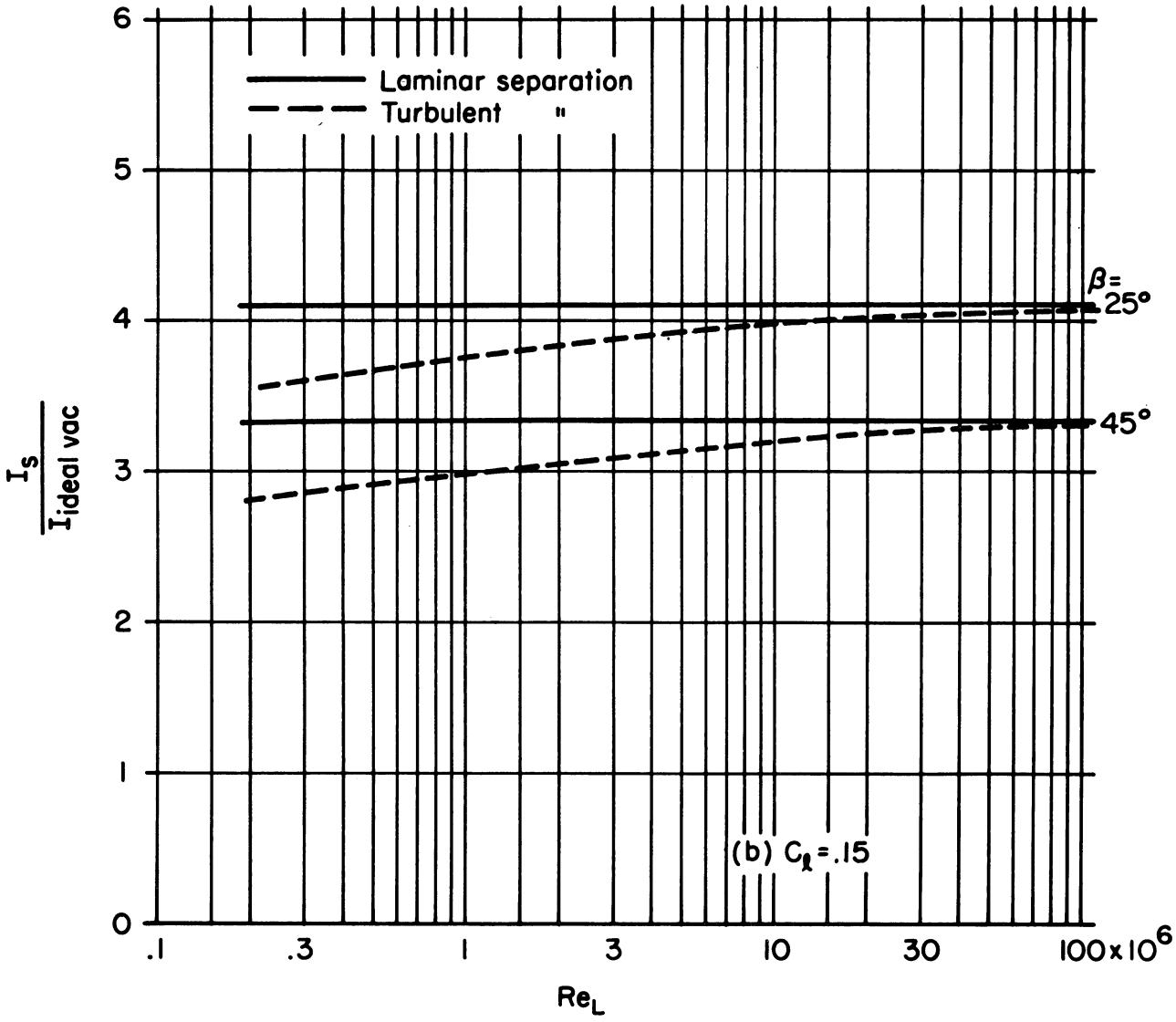

Figure 14. Concluded.

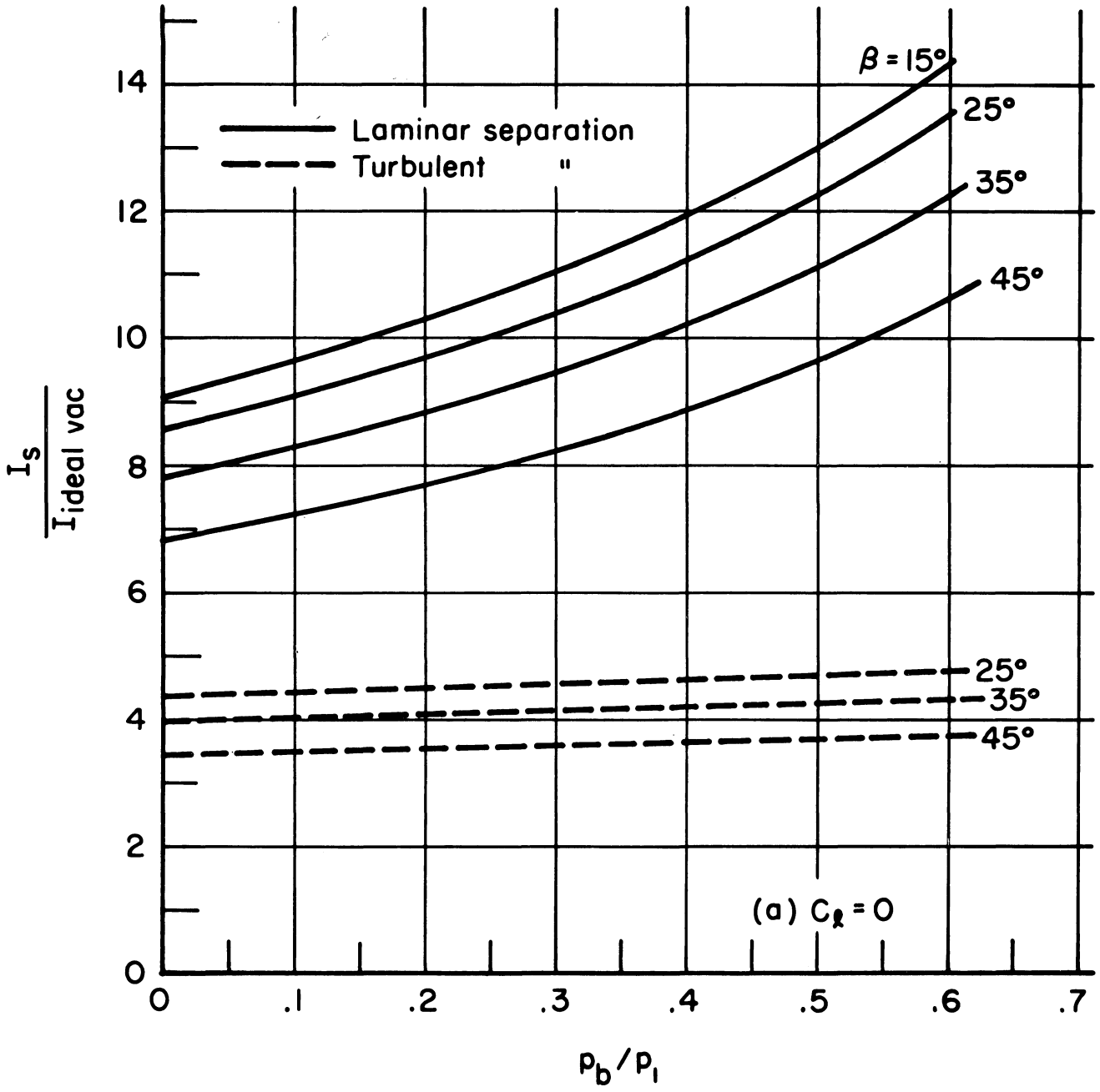

Figure 15. Specific impulse vs. base pressure for $M_1 = 8.0$ and $\delta = 90°$. $M_j = 8.0$, $\gamma = 1.4$, $Re_L = 10^7$.

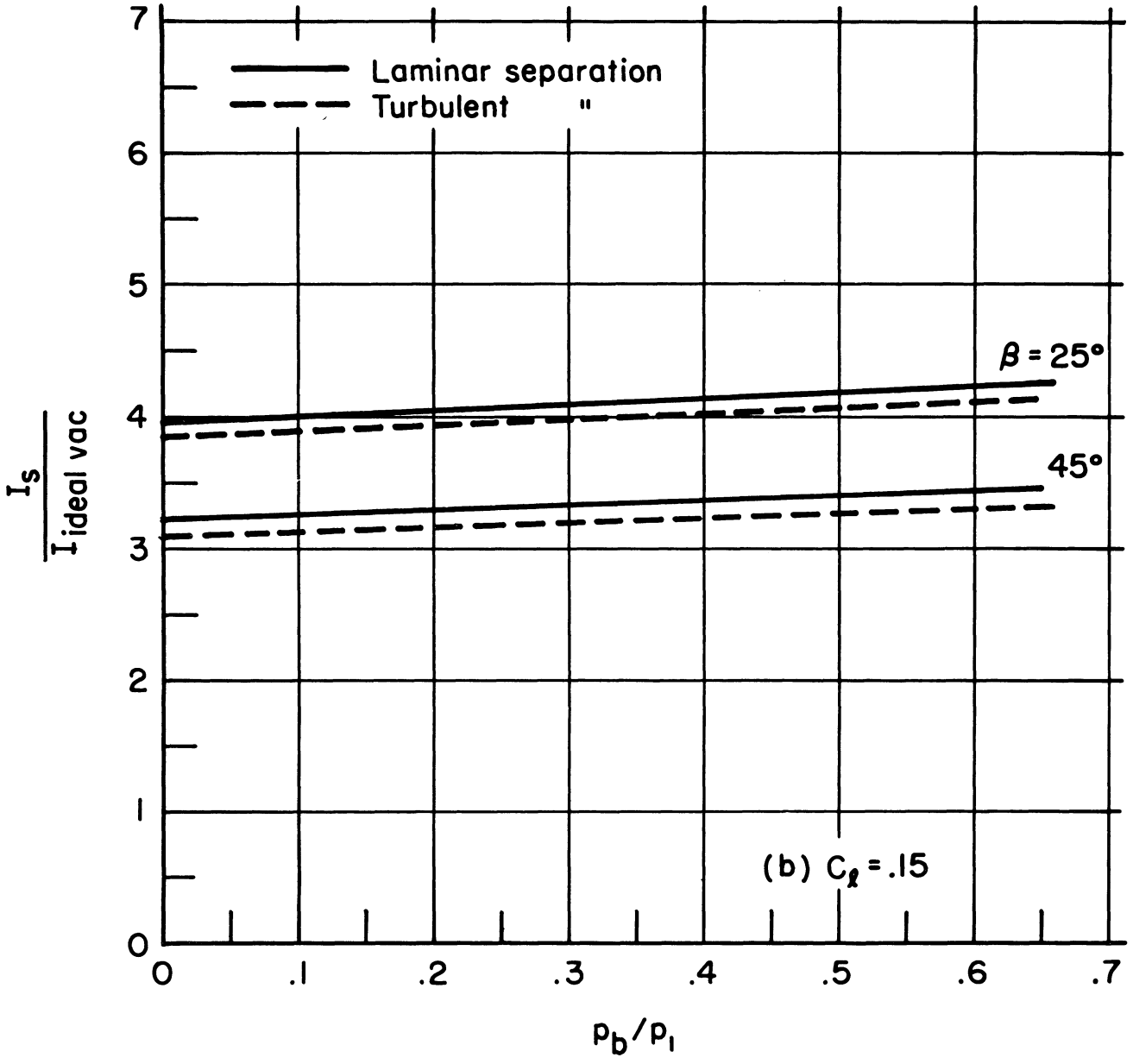

Figure 15. Concluded.

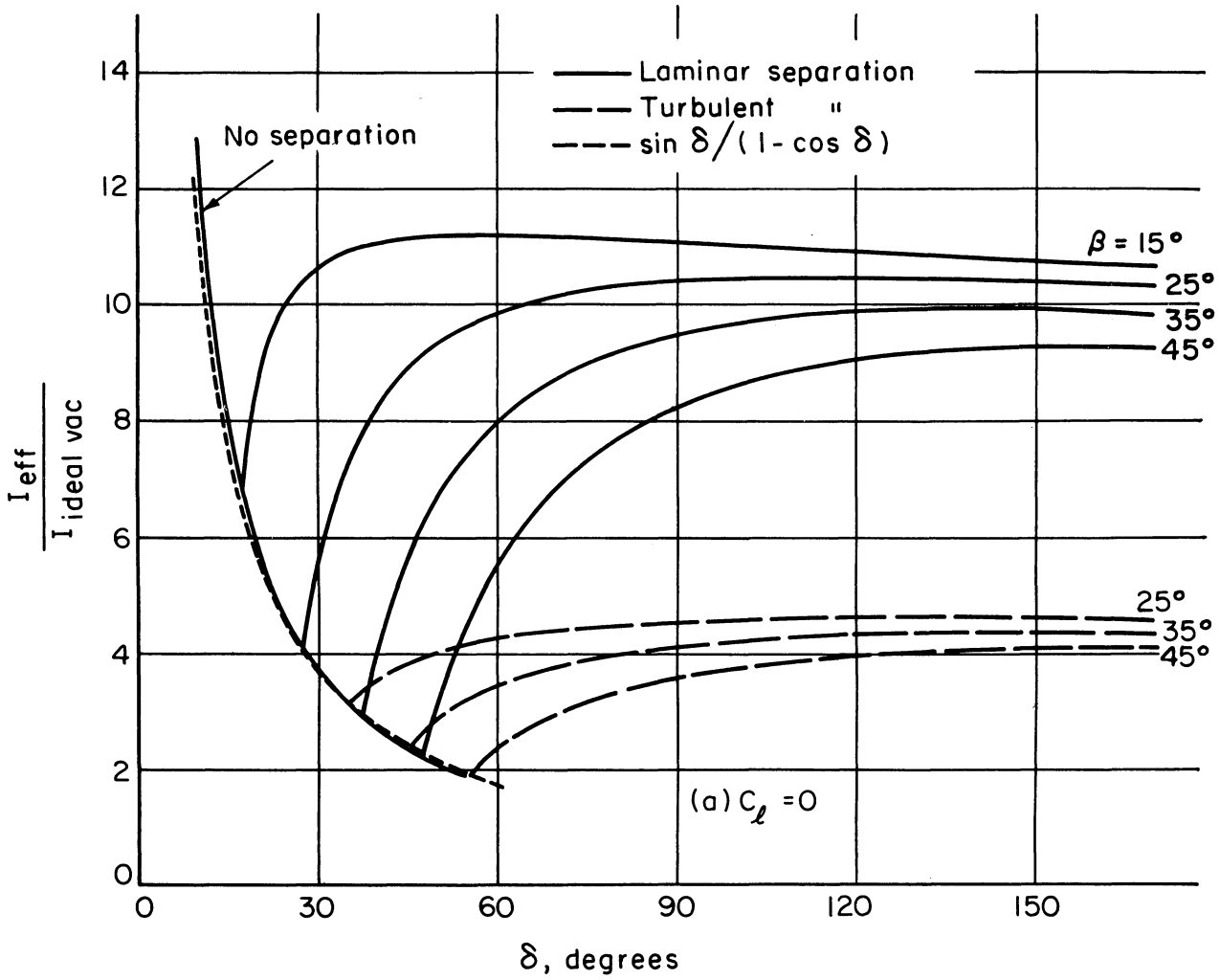

Figure 16. Effective specific impulse vs. jet-flap deflection angle δ for $M_1 = 8.0$. $M_j = 8.0$, $\gamma = 1.4$, $p_b/p_1 = .3$, $Re_L = 10^7$.

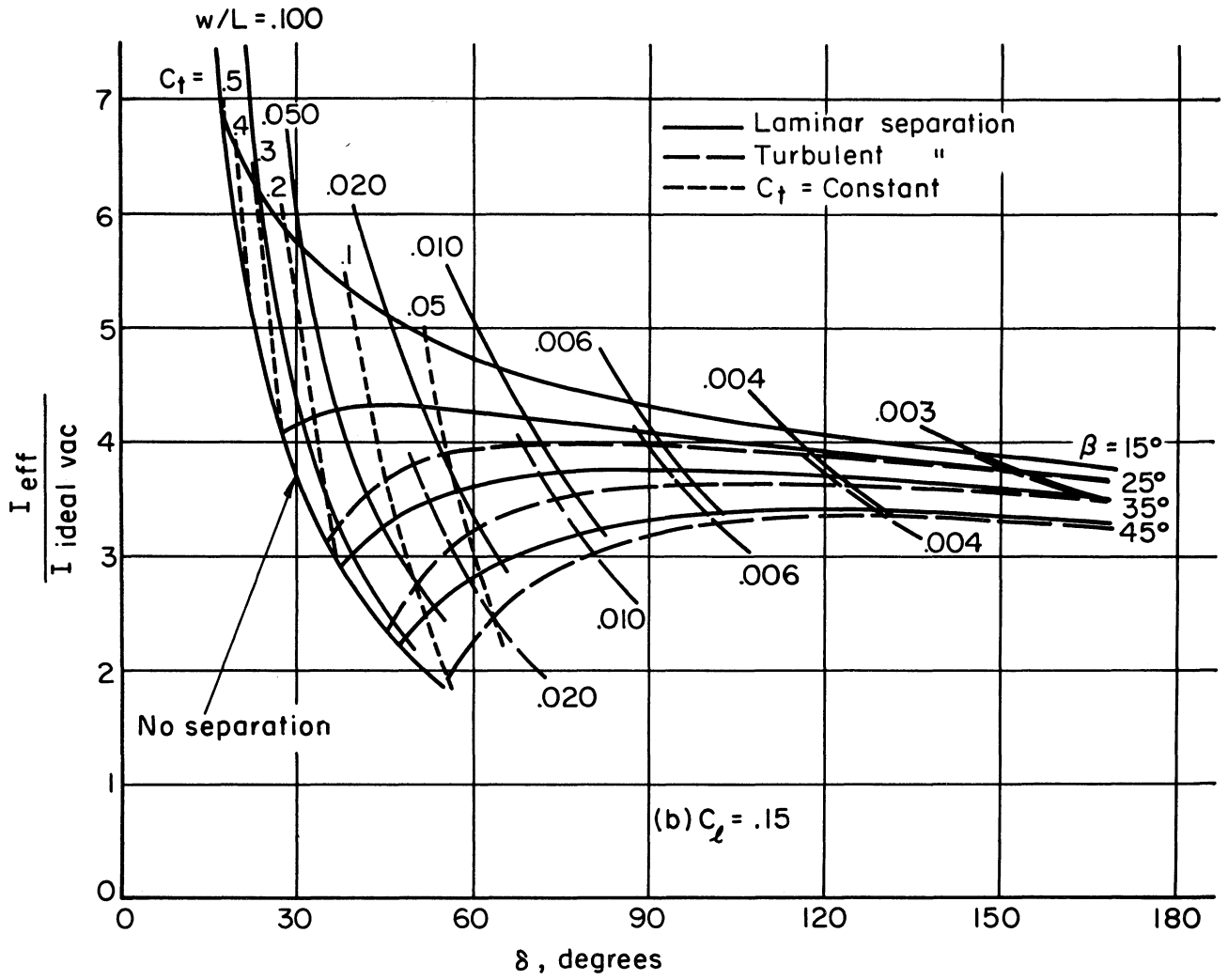

Figure 16. Concluded.

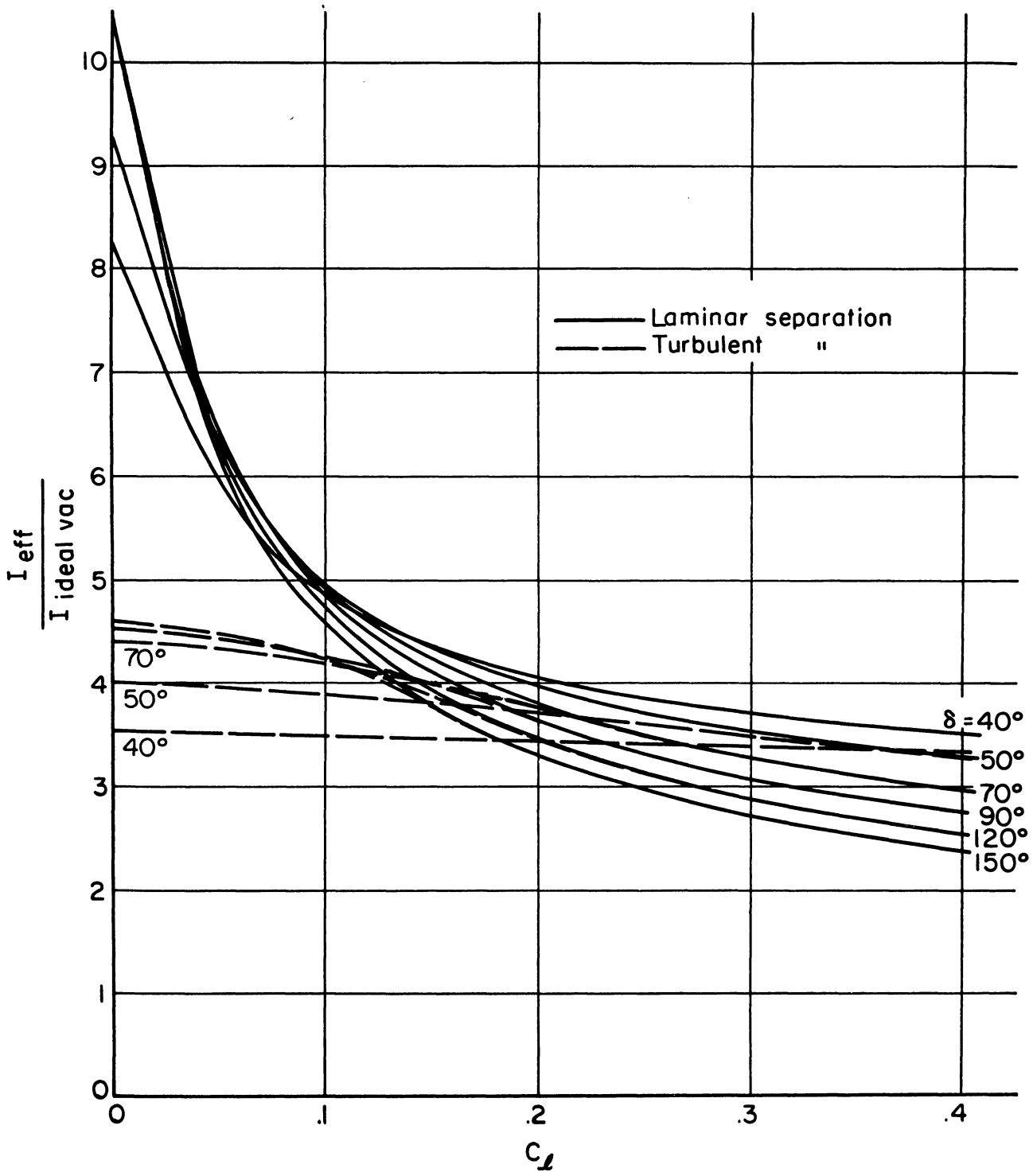

Figure 17. Effective specific impulse vs. section lift coefficient for $\beta = 25°$ and $M_1 = 8.0$. $M_j = 8.0$, $\gamma = 1.4$, $p_b/p_1 = .3$, $Re_L = 10^7$.

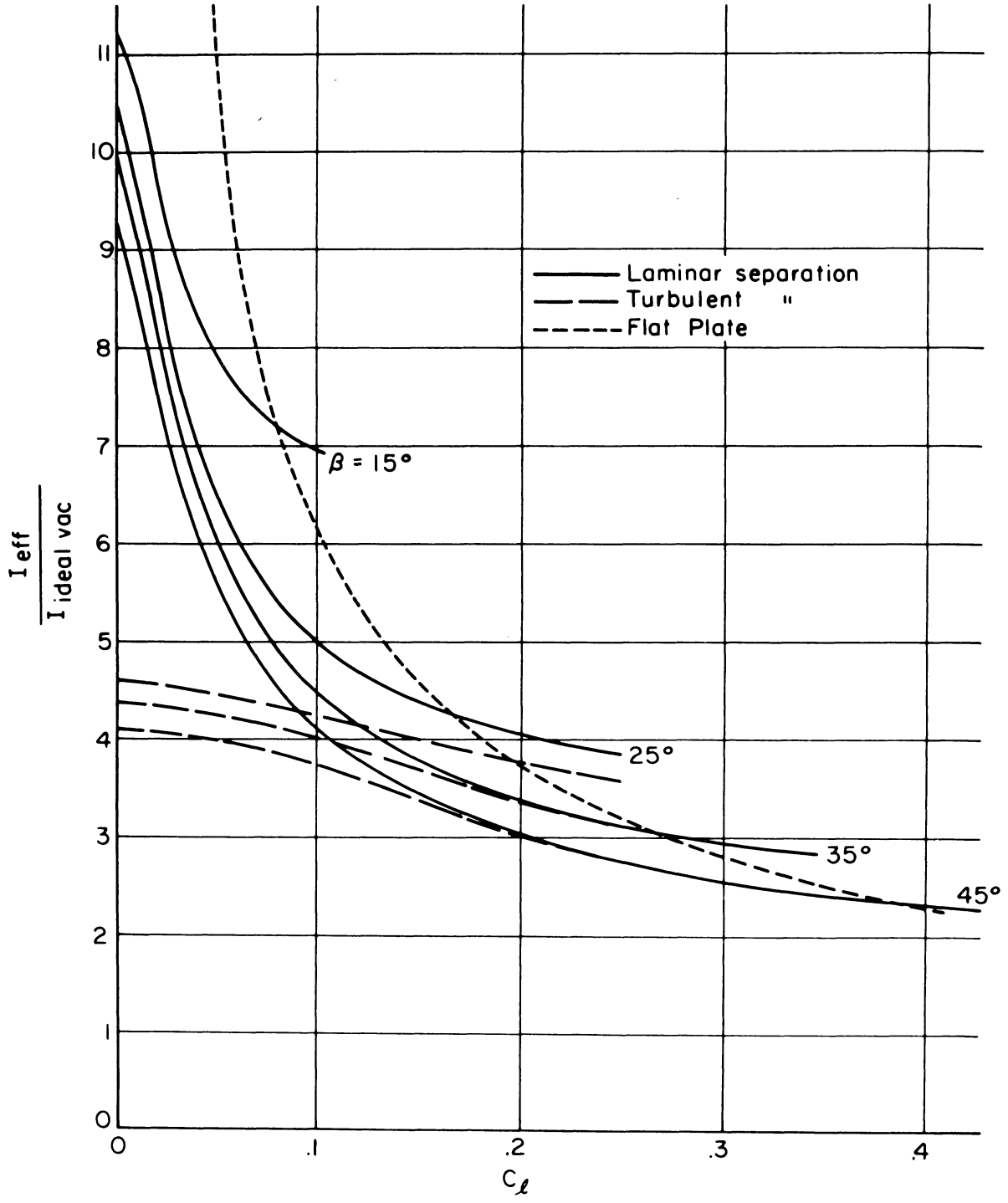

Figure 18. Effective specific impulse vs. section lift coefficient for optimum flap deflection angles at $M_1 = 8.0$. $M_j = 8.0$, $\gamma = 1.4$, $p_b/p_1 = .3$, $Re_L = 10^7$.

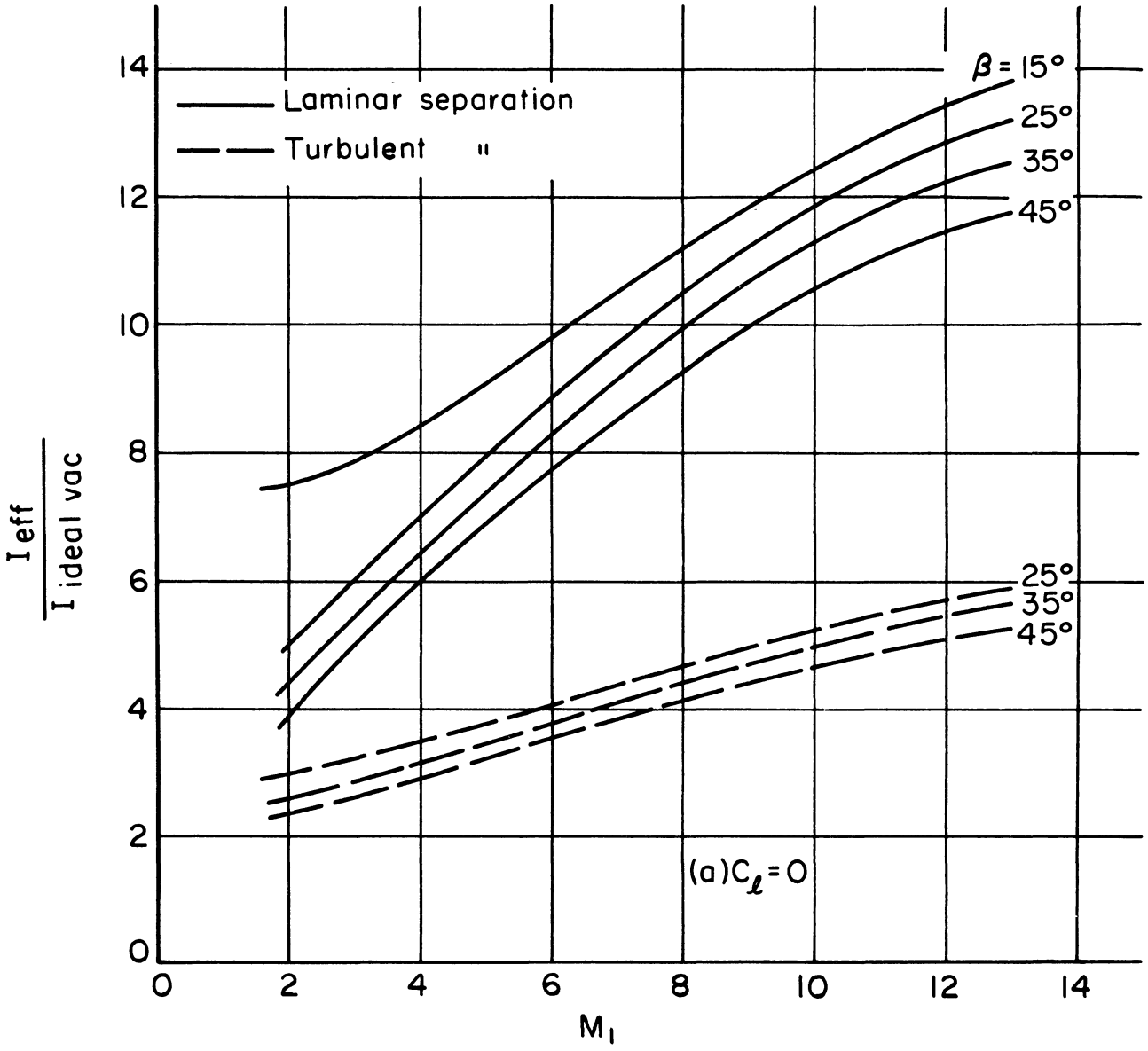

Figure 19. Effective specific impulse vs. free-stream Mach number for optimum flap deflection angles. $M_j = 8.0$, $\gamma = 1.4$, $p_b/p_1 = .3$, $Re_L = 10^7$.

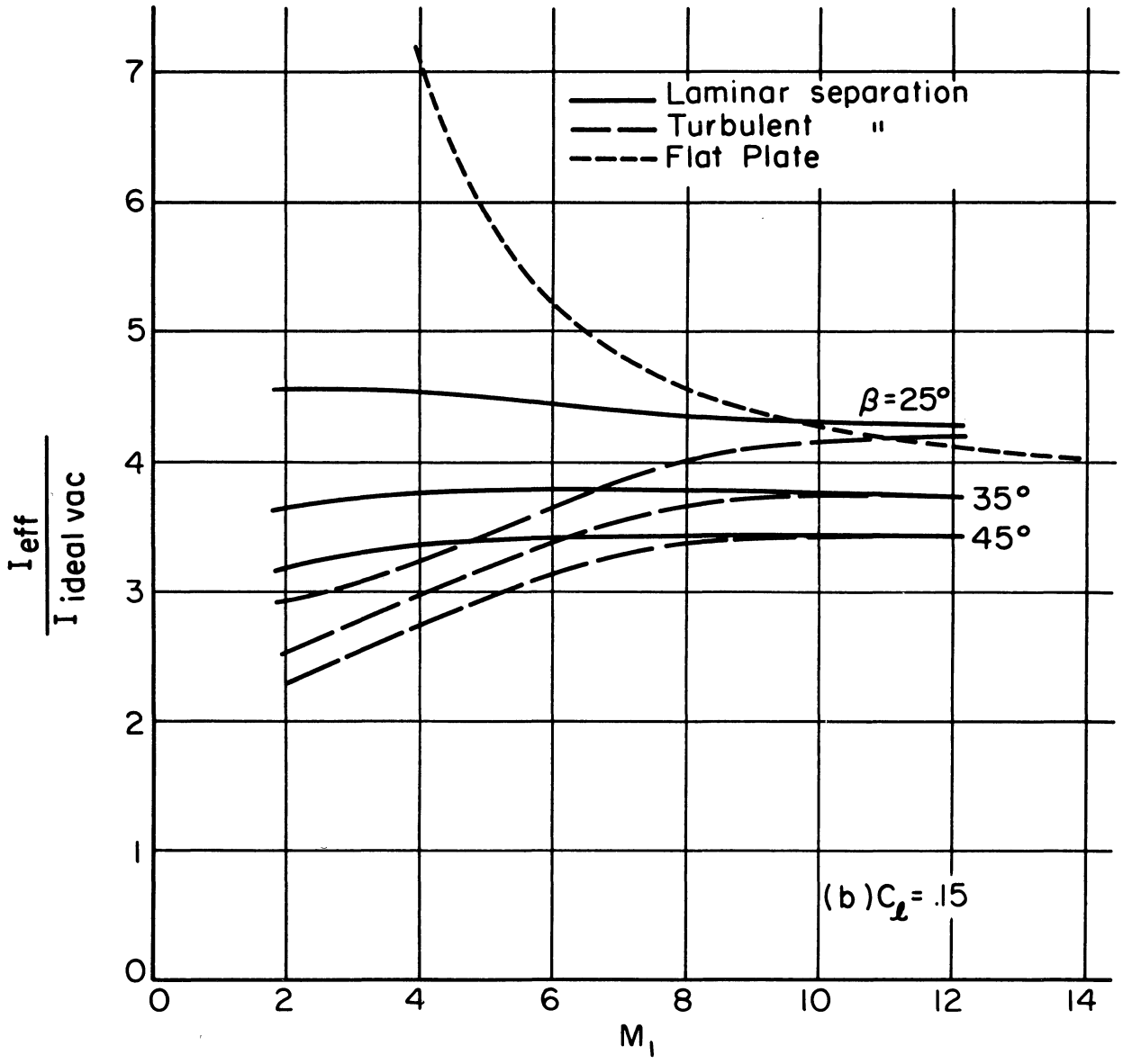

Figure 19. Concluded.

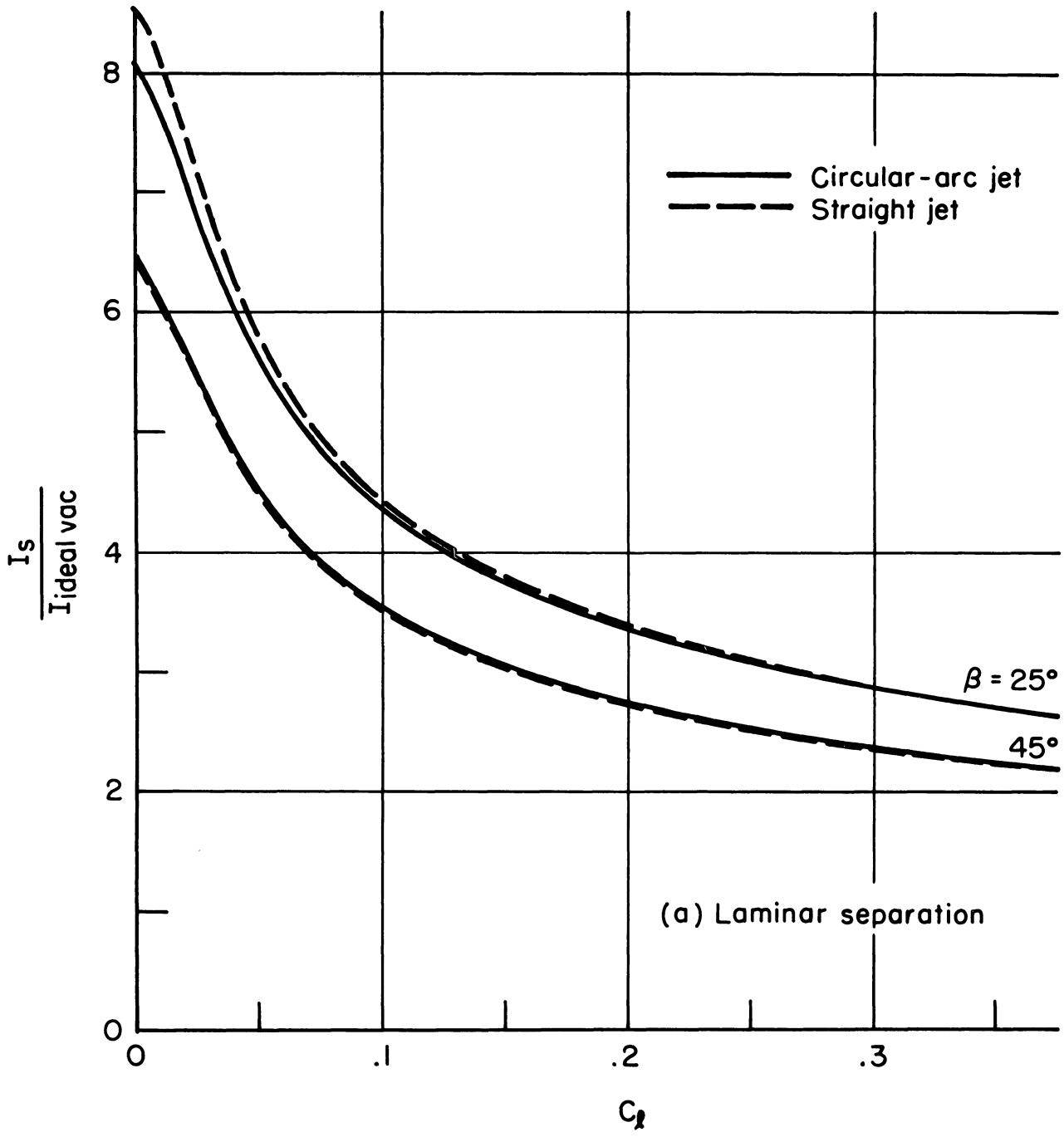

Figure 20. Specific impulse vs. section lift coefficient for straight jet flaps and for circular-arc jet flaps, at $M_1 = 8.0$ and $\delta = 90°$. $M_j = 4.0$, $\gamma = 1.4$, $p_b/p_1 = 0$, $Re_L = 10^7$.

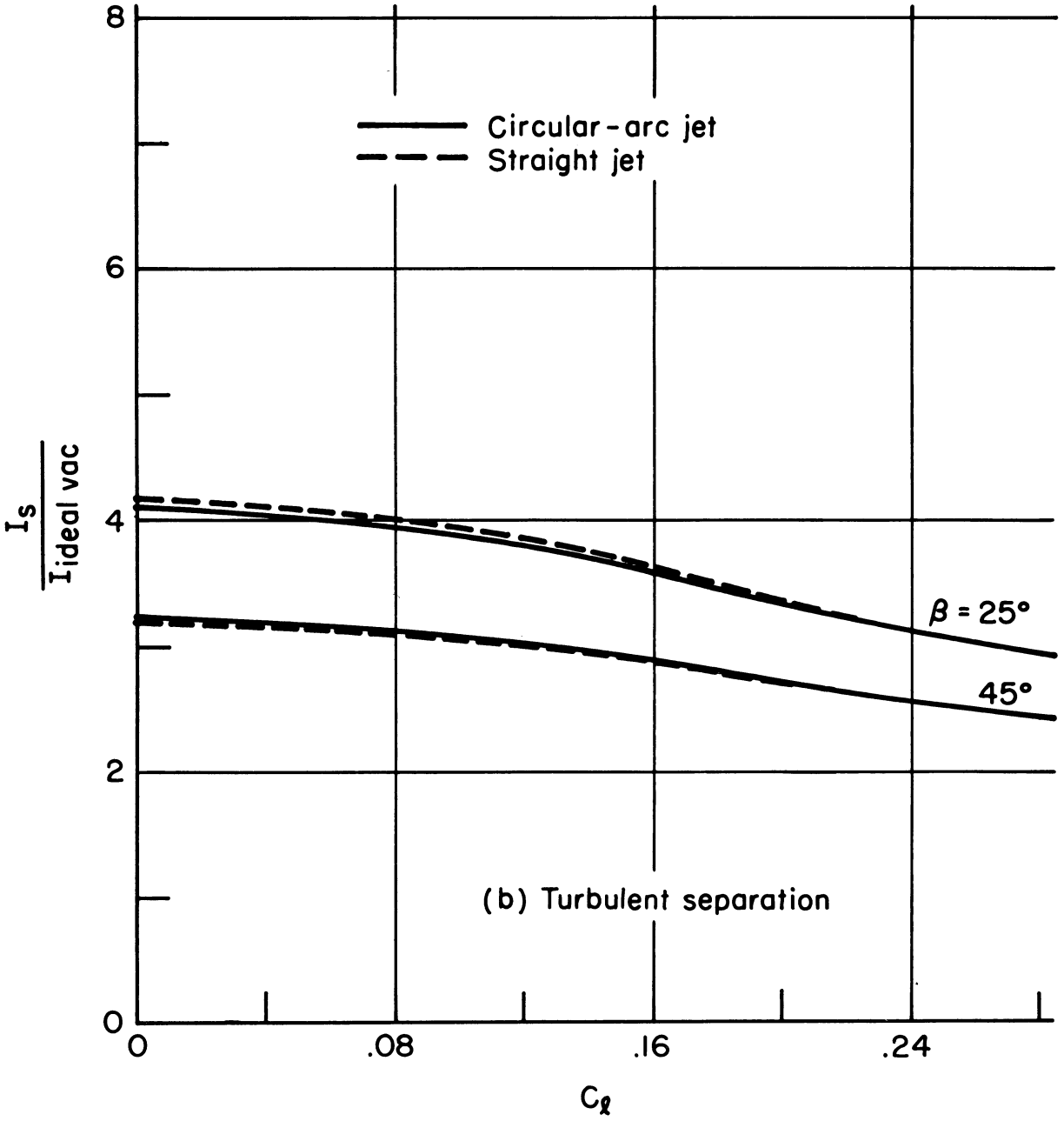

Figure 20. Concluded.

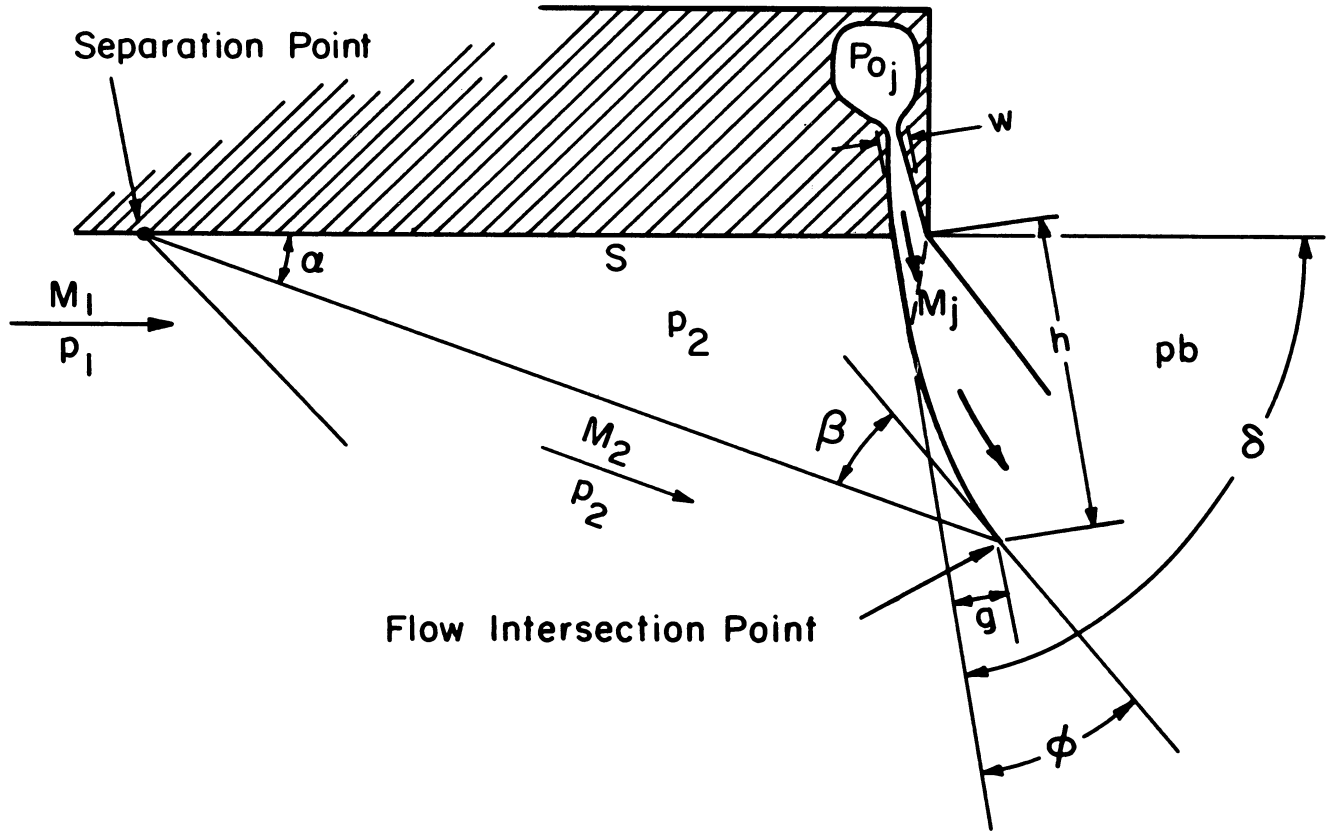

Figure 21. Two-dimensional straight jet-flap flow model.

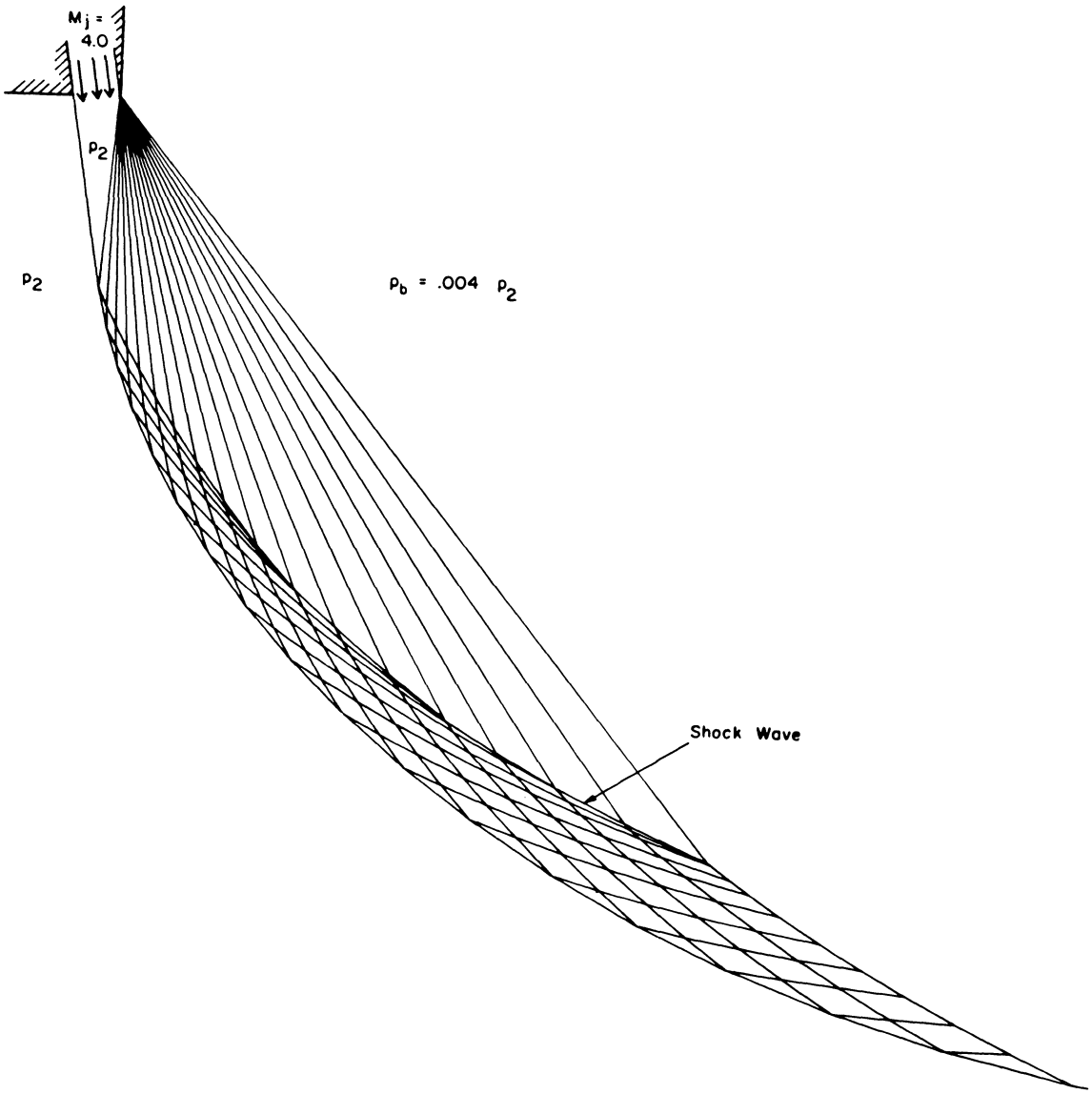

Figure 22. Jet shape determined by method of characteristics for irrotational flow.